A Computational Framework for Predicting the Adhesion Strength of Bonding in Cold Spray

by

Amir Arsalan Khoei

A thesis

presented to the University of Waterloo

in fulfilment of the

thesis requirement for the degree of

Master of Applied Science

in

Mechanical and Mechatronics Engineering

Waterloo, Ontario, Canada, 2023

Author's Declaration

I hereby declare that I am the sole author of this thesis. This is a true copy of the thesis, including any required final revisions, as accepted by my examiners.

I understand that my thesis may be made electronically available to the public

Abstract

In recent years, Cold Spray technology has proven to be a promising method of powder deposition in surface coating and additive manufacturing applications. This process is done without melting the particles prior to deposition; therefore, a wide range of materials can be deposited onto a substrate through the powder's kinetic energy. In contrast to traditional coating methods, in CS the particle temperature remains below its melting point. As a result, the adverse effects of melting and other temperature-related defects are avoided in CS. The kinetic energy needed for successful bonding is characterized by a powder's critical velocity that is dependent on the properties of the powder material. The quality of the cold sprayed coatings depends strongly on the adhesion strength at the particle-substrate interface. Predicting the adhesion strength thus plays a crucial role in optimizing the process parameters of CS process to achieve desired surface coating qualities.

Utilizing numerical approaches, to study the occurrence of bonding in CS and observe the material jetting phenomena due to bonding, is more convenient than using empirical approaches. Experimental observation of particle bonding in CS is inherently very difficult due to the extremely small time and length scales at which particle bonding happens in CS. Numerical modeling has thus been an indispensable tool in the study of CS. Most numerical studies on CS have focused on using the traditional mesh-based FEM, which often face limitations when modelling the extreme plastic deformation occurring during particle impact. In comparison, meshless methods are proven to perform significantly better as they resolve the issue of mesh distortion in mesh-based methods Furthermore, majority of existing models are only able to model the impact and bonding processes and very few methods exist that can predict the bonding strength accurately.

In the present work, a computational method is proposed for modeling bonding of powder particles in cold spray capable of predicting the adhesion strength. The method relies on a bonding model developed in previous research [1, 2] which is based on the commonly held view that bonding occurs due to large plastic strains occurring at extreme rates. This is achieved by introducing a strain-like history variable named *bonding parameter* and two material constants, the critical surface adhesion energy, and the critical surface adhesion energy rate. In this thesis, the bonding model is complemented with a semi-empirical evolution law for adhesion strength on bonding boundaries. The strength evolution model interacts with the bonding evolution model and is coupled with the bonding parameter.

The model is implemented numerically within a material point method (MPM) in a way that effectively eliminates spurious mesh dependence and captures complex phenomena such as jetting. The adhesion strength model proposed in this study utilizes the direct bonding model results and fundamentals from our previous study [1, 2]. The adhesion strength model proposed here is then used to predict adhesion strength and study the case of single particle impacting a substrate.

In doing so, the distribution of adhesion strength will be shown through the contact region. The model parameters are also discussed, and it will be shown that how the change of these parameters will affect the adhesion strength. In previous studies the average adhesion strength values were achieved from experiments. The values for the average adhesion strength will also be highlighted in the present numerical study.

The simulations were performed for pure Aluminum (99.7%) particles impacting Al substrate. The chosen material is similar to previous research works and studies. Further into the thesis the adhesion strength model will be discussed, and corresponding results will be discussed afterwards. According to the results obtained, the average adhesion strength for a single pure Al powder (14 micro-meter diameter) impacting an Al substrate at 810 m/s (which is approximately the critical velocity) is predicted to be 42.16 MPa. The corresponding critical adhesion energy and energy rate used were 1500 J/m^2 and 2 $J/m^2 s$ (these will be discussed later in the thesis), which are also approximately near the calibrated values. Results are very encouraging and exhibit desirable agreement with known experimental data such as critical bonding velocity, adhesion strength, and deformed particle/substrate shape.

Acknowledgments

Table of Contents

List of Figures

List of Tables

List of Abbreviations

ASI: Adiabatic Shear Instability

CS: Cold Spray

DED: Direct Energy Deposition

FATSLAB: Fatigue and Stress Analysis Laboratory

FEM: Finite Element Method

FEA: Finite Element Analysis

JC: Johnson-Cook

MPM: Material Point Method

MUSL: Modified Update Stress Last

PTW: Preston-Tonks-Wallace

RMS: Root-Mean-Square

SEM: Scanning Electron Micrography

SPH: Smoothed Particle Hydrodynamics

TS: Thermal Spray

USL: Update Stress Last

USF: Update Stress First

List of Symbols

b: Body force per unit

D_{bond}: Bonding Parameter

$DCell$: Grid Cell Spacing

dp: Particle (material point) Spacing

f: Force

$\emptyset$: Shape Function

G_c: Critical Surface Adhesion Energy

$\dot{G}_c$: Critical Surface Adhesion Energy Rate

G_{bond}: Adhesion energy for bonding

K: Tuning parameter

κ: Threshold for D_{bond}

m: Mass

P: Pressure

R: Radius

ρ: Density

σ: Stress

σ_c: Maximum Bonding Stress

σ_{vm}: Von-Mises stress

V: Velocity

$\Delta\varepsilon_p$: Increment of Effective plastic strain

ΔG_s: Increment of Adhesion Energy

Chapter 1: Introduction

1.1.   Cold Spray Technology

Cold Spray (CS) (also known as supersonic particle deposition) is an innovative Additive Manufacturing (AM) process that involves the deposition of metal, ceramics and/or composite powders onto substrate. As depicted in Figures 1.1 – unlike traditional AM techniques – CS is a solid-state process in which microparticles are speeded up, to reach supersonic speeds (Mach 2-3) [3] using a de Laval nozzle and a stream of compressed gas including helium or nitrogen. Compared to other AM methods, CS offers several advantages:

1. Low heat input: Since CS does not involve melting the powder material, it can be used with temperature-sensitive materials that may be prone to distortion or chemical changes when exposed to high temperatures. This allows the use of a wide range of materials, including metals, ceramics, and composites. Additionally, there will be no intermetallic formed at the interface of coating and substrate.
2. Dense and pure coatings: The high-velocity impact of the powder particles during cold spray promotes minimal porosity in the deposited coatings. This leads to coatings with excellent mechanical properties, such as high hardness and improved wear resistance.
3. High Throughput: Cold spray achieves high material utilization rates, as most of the powder particles impact and adhere to the substrate. This results in minimal material waste and cost-effective production.
4. Minimal thermal stress: As cold spray does not involve significant heating or cooling, it reduces the risk of thermal stress-induced deformation, making it suitable for additive manufacturing of large and sensitive parts.
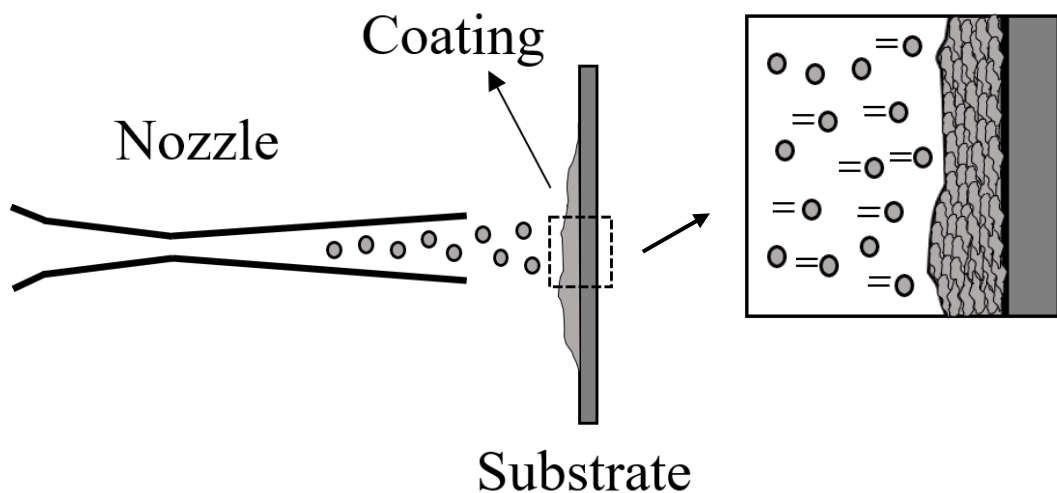
Figure 1.1 Schematic of Cold Spray System

When comparing CS to Thermal Spray both utilize similar coating materials. The primary limitation lies in the particle size of the powder that can be sprayed, with CS is capable of applying significantly finer particles, including nanocrystalline powders. One significant limitation of TS is that it necessitates high temperatures for effective bonding with the substrate, posing challenges and impossible to use in a sealed setting. Considering CS disadvantages, the process resolution is constrained by the size of the "spray spot," typically measuring several millimeters. Furthermore, the intense plastic deformation of the particles can result in the accumulation of residual stresses within the deposited material, potentially causing distortion, deformation, or the formation of cracks.

Numerical simulation plays a crucial role in the understanding, optimization, and advancement of the cold spray (CS) process. It involves using computational models and simulations to predict and analyze the behavior of particles on impact during CS process. Following are some key reasons why numerical simulation is important for CS:

1. Process optimization: Numerical simulations allow the study of different process parameters, such as gas velocity, temperature, particle size, and substrate material, to optimize the CS process. By simulating various scenarios, it can identify the optimal conditions for achieving desired coating properties, such as bonding strength, thickness, and porosity. This helps in reducing experimental trial and error, saving time, and resources. [4]

2. Predicting coating microstructure: The microstructure of the deposited coating significantly influences its mechanical properties. Numerical simulations can predict and help in understanding how process parameters affect microstructural evolution, e.g., occurrence of dynamic recrystallization, and enables the design of coatings with desired mechanical and thermal properties. [5]

3. Scale-up and process design: Numerical simulations are valuable for scaling up the CS process from laboratory-scale to industrial-scale applications. By simulating larger deposition volumes, researchers can assess the feasibility of scaling and identify potential challenges, such as gas flow distribution, particle entrainment, or pressure losses. This information guides the design of efficient CS systems and helps in ensuring successful implementation in production environments. [6]

4. Cost and time savings: Experimental investigations in cold spray can be time-consuming, costly, and limited by the availability of materials and equipment. Specifically, the impact of particles, and corresponding deformation happens over a nano-to micro-seconds period and therefore hard to capture experimentally. Numerical simulations provide a cost-effective and efficient alternative for exploring different process configurations, optimizing parameters, and predicting outcomes. This reduces the number of physical trials required, accelerates process development, and ultimately saves time and resources. [7]

The adhesion strength of the deposited coating is a critical factor in determining its performance and durability. A reliable numerical model can help optimize process parameters to achieve the desired adhesion strength. The adhesion strength prediction model allows for the assessment of

different material combinations and their compatibility with the substrate. This helps in selecting the most suitable materials that will provide the desired adhesion strength for specific applications. Recent studies mainly focus on achieving bonding in CS, but being able to predict the adhesion strength in the case of bonding was not the main goal of the studies. This study focuses on proposing a numerical model capable of predicting the adhesion strength in bonding conditions.

1.2.   Thesis Motivation and Objectives

In CS process and the coatings achieved from this technology, the importance of bonding was always noteworthy in previous research. The bonding phenomenon has always been on the issue of how and when it occurs [2, 3, 5, 6]. In our research group's previous research [1, 2], similar studies on the bonding model were studied and analyzed using a novel particle-based method, known as the Material Point Method (MPM). In the mentioned study, the importance of bonding, the bonding phenomenon, and the methods for modeling the bonding was discussed. However, the prediction of bonding strength was not addressed. Without a reliable numerical model, it becomes challenging to predict the adhesion strength of the deposited coatings. This can result in inconsistent coating quality, with variations in adhesion strength from one production run to another. Inadequate adhesion can lead to coating failures, such as delamination or premature wear, compromising the performance and reliability of the coated components. On the other hand, the ability to predict adhesion strength through numerical modeling provides a means of quality control during the CS process. By comparing the predicted adhesion strength with desired specifications, the quality of the deposited coatings can be assessed in real-time. This allows for the identification of potential issues or process deviations, enabling timely adjustments and ensuring consistent coating quality.

This study goal is to develop a methodology for predicting the adhesion strength in CS bonding, addressing the research gap in numerical modelling of CS bonding. To achieve this goal, following objectives are pursued:

- Establish a methodology for predicting adhesion strength using an energy parameter that includes strain/strain-rate, as the main predictor of adhesion, and stress/stress-rate as the main predictor of strength.
- Develop a numerical framework, using MPM, for predicting the adhesion strength
- Verify the developed framework
- Implement the developed framework for predicting CS of pure Al powder (99.7%) particles on Al substrate adhesion strength

1.3.   Thesis Outline

This thesis consists of six chapters. Chapter 1is on motivation, importance, goal, and objectives of this research. Chapter 2 gives a comprehensive review of previous studies. In the mentioned chapter, adhesion and its phenomena in CS are discussed and the importance of adhesion strength is highlighted. Chapter 3 provides the background of the numerical modeling of CS adopted in this research. The use of Material Point Method in this study and its validation will

be discussed. In Chapter 4 the direct bonding model and the proposed adhesion strength bonding model will be discussed in detail and the adhesion strength in the bonding phenomenon will be presented from both numerical and experimental viewpoints. In Chapter 5, the results of the developed numerical model for adhesion strength prediction will be presented, verified, and discussed. Finally, Chapter 6 presents conclusions from highlights of the presented work and explores potential future research directions.

Chapter 2: Literature Review

In recent years many studies and observations have been made on the CS process and how process parameters in CS can affect the result of coatings (whether achieved or not). These studies were done utilizing both empirical and numerical approaches, but little study, if any, has been done on the prediction of the adhesion strength in CS.

CS technology is applied in various fields, such as aerospace, automotive, and electronics [8, 9]. To restore valuable metal components that have been damaged, traditional methods like arc welding, thermal spraying, and laser deposition are commonly employed. However, these conventional techniques often lead to significant flaws due to excessive heat and high temperatures. Examples of such defects include oxidation inclusions, thermal deformation, and cracking, which can greatly limit the effectiveness of the repairs. Additionally, certain delicate components with intricate shapes are impractical to repair using the aforementioned methods, resulting in their disposal and a substantial waste of resources and energy. In contrast, cold spray technology possesses a unique characteristic of solid-state deposition. This feature allows it to mitigate the defects associated with excessive heat and high temperatures. Consequently, cold spray technology holds considerable potential for use in the repair of aerospace, naval, and automotive components [8].

CS is used for a range of purposes, such as corrosion protection [10, 11]. Mohammad et al. [11] observed the corrosion fatigue of aluminum powder sprayed on AZ31B. The AZ31B alloy with cold sprayed Al coating resulted in significant protection from corrosion attack. The main factors of outstanding corrosion performance were identified as strong adhesion of the coating as well as the porosity of Al coating being very low. The tests were also performed in corrosive environment (3.5% NaCl) which significantly influenced the fatigue life of coated and non-coated samples of AZ31B. The fatigue life of both sample conditions decreased due to the fracture of oxide layer at the tip of the crack – low ultimate tensile strength of pure aluminum – caused by plasticity.

Other uses of CS are in wear resistance [12], repair of damaged or worn-out components [13], and thermal barrier coatings [14]. Research and development in CS technology continues to explore new materials and process optimization techniques [15]. CS is a versatile coating deposition process with numerous applications across various industries. Its advantages, such as low-temperature operation, high bond strength, and versatility in material selection, make it an attractive option for coating, repair, and surface modification needs.

Considering a previous review study by Wenya Li. et. al. [16], the mechanisms behind the bonding and impact in CS at high particle velocity were analyzed from both numerical – in particular finite element method – and empirical aspects. The study stated that numerical simulations explore particle bonding and deformation reasonably as well as correspond to experimentally observed behavior. It was also mentioned that the numerical simulations offered various information during the impact process such as particle deformation morphology, material jetting, temperature, stress, and strain.

Considering the achieved information from numerical simulations in CS during impact, fewer studies delve into the observation of adhesion strength in bonding conditions. This Chapter consists of a review of previous studies and their applications on CS. The bonding phenomenon and the importance of having knowledge on the adhesion strength in the contact zone will be reviewed.

2.1. Cold Spray Study and Application

Over the past few years, it has been evident that cold gas spraying is a promising powder deposition method which utilizes kinetic energy, rather than thermal energy, from a particle deposited at a critical velocity to achieve a solid-state deposition. This process in cold spray ensures that undesirable thermal effects which might occur due to melting are eliminated and quick deposition is done at its highest efficiency. The coatings from the deposition indicate high strength and hardness. The coating also shows high bonding strength with the substrate which improves the cyclic performance of the coated part [17]. In a previous study by Ghelichi et al. [18] it was shown that the fatigue strength of CS treated parts was significantly increased (up to 30%) for coated parts. Al5051 specimens were used and were sprayed by Al7075 feedstock powder. The coated parts were stronger components and had much higher fatigue endurance, indicating higher bonding strength, in comparison to regular parts.

The critical impact velocity of powders in cold spray identifies whether bonding has occurred or not and has a unique value for set of known processing and material parameters. The critical velocity is dependent on several factors such as particle size, oxide layer thickness, particle and substrate materials being paired, and impact temperature. Li et. al. [19] estimated the critical impact velocity of copper (Cu) both experimentally and theoretically. Their study results showed that the critical velocity changed with the oxygen content and particle temperature. The higher the particle temperature, the lower the critical velocity became.

In CS, it is important to maintain the temperature below the melting point. There are two reasons for this matter: first, the deposition will occur at a high rate and more effectively, and second thermal defects will be eliminated [1]. It should be kept in mind that in modern CS it is not clear whether powder remains in solid state upon impact or not. Schoop [20] highlights that the particles and the substrate in case of not using a converging-diverging nozzle "welded together". Not using a converging-diverging nozzle prevents the particles acceleration to the critical velocity and this shows that melting or partial melting was involved in impact.

Although deposited coatings do not have an innate strength or hardness, they manifest bond strength with the substrate. This property can generally enhance the performance of the coated segments. The bonding strength (namely, adhesion strength) of sprayed materials is a crucial factor in the mechanical properties of the coating. Establishing a relationship between CS process parameters and the bonding strength enables optimizing the CS process and achieve desired properties.

Studies on resistant coating should also be mentioned, the CS impact process causes the effect of work-hardening on the material which induces residual stress and increases its fatigue strength [14]. The presence of residual stresses in the cold-sprayed coatings can affect their mechanical properties, such as adhesion, cohesion, and fatigue resistance. Residual stresses can also influence the performance and longevity of the coated component. Kelvin Loke [21] analyzed the residual stress of Al6061 powders at different angles from numerical approach. In comparison to empirical observations, the results achieved from numerical approach seemed similar, and it was observed that the bonding region decreased with the increase of spray angle.

2.2. Cold Spray Bonding Theory

For the oxide layer to be removed both the powder particles and the substrate should go under sever plastic deformation. CS utilizes contact pressure and kinetic energy (rather than thermal energy) for the breakage of the oxidation layer from the substrate. This process results in fresh metal-to-metal contact at the bonded interface. The high contact pressure will cause bonding to occur due to metallurgical bonding and mechanical interlocking [2]. Successful bonding normally requires critical velocity that might reach 800 m/s or more in many cases. All of the impact and bonding process occurs within nanoseconds, making it extremely difficult for experimental observation. Therefore, use of numerical modelling has been the for front of adhesion studies of CS bonding.

Beside mechanisms such as oxide layer break-up [22], other mechanisms such as localized melting [23], and mechanical interlocking have been proposed as the underlying mechanisms of bonding phenomenon, none of these methods have been conclusively proven to explain bonding although they have been supported partially by experimental observations. Nonetheless, formation of an out-flow jet of materials in the contact zone is commonly believed to provide enough strain deformations for successful bonding to occur. Formation of the outward jet is often referred to as jetting and is considered to characterize successful bonding.

Figure 2.1 shows a Scanning Electron Micrography (SEM) image of a gold particle impacting a gold substrate at 375 m/s [22]. Figure (a) represents the top view of the bonded particle. The formation of the outward material jet, namely the material jetting can be seen in periphery of the bonded area. White line in Figure (b) represents the top surface of the particle. The formation of the jet can be seen on the edges of the contact area. Figure (c) represents a magnified look at the contact region of the particle and the substrate. It can be seen that the contact area consists of both bonded regions caused by the metallic bonding, as well as non-bonded area, namely the gap. The observed contact region was also achieved in this thesis study and will be discussed in detail in the upcoming chapters.
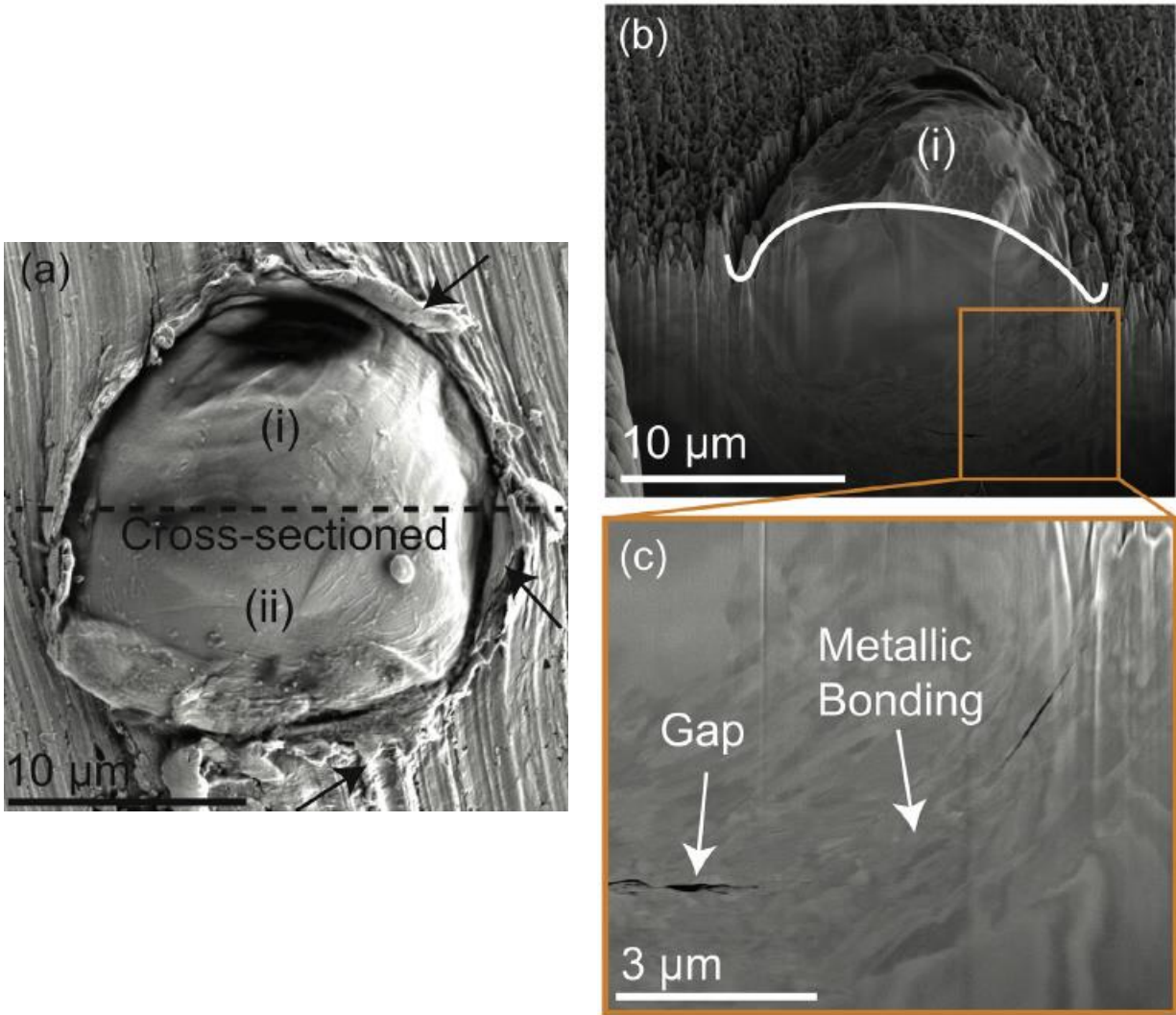
Figure 1.1 SEM image of gold particle impacting gold substrate. Figure (a) shows the contact formation and material jetting from top view. Figure (b) represents the top surface of the particle with white line. Figure (c) shows a closer look at the contact region. [22]

In earlier works, Assadi et al. [24], suggested Adiabatic Shear Instability (ASI) as the main cause of jetting at contact zones. It was mentioned that bonding occurs due solely to kinetic energy during impact, and successful bonding occurs if the particle velocity is above its critical value. This value was mentioned to be dependent on temperature and thermomechanical properties feedstock material. ASI was described as the adiabatic heating generated at the contacted zones softens the material, without melting, reducing its load bearing capacity. Consequently, the material in this region behaves like a fluid which results in material fragmentation and jetting. Figure 2.2 represents the simulation impact of the particle utilizing Finite Element Method. The jetting formation of the copper particle impacting the copper substrate can be seen. The initial velocity of the particle is 600 m/s and the contours represent the temperature distribution.
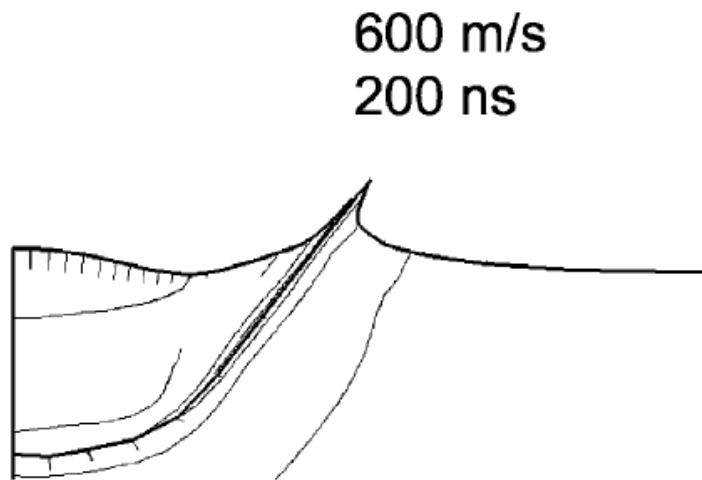
600 m/s
200 ns

Figure 2.2. Simulation of copper Particle impacting copper substrate. The initial velocity is 600 m/s. The arrows define velocity of surface nodes during impact.

Figure 2.3 shows a three-dimensional simulation of two gold particles impacting the gold substrate reported in [24]. The jetting formation was observed to be the cause of temperature and heat generated during impact.

15 ns
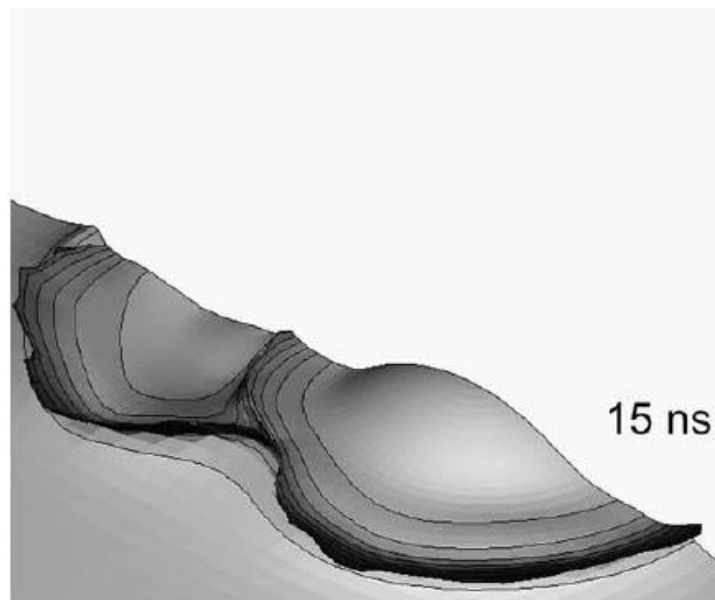
Figure 2.3. 3D simulation of two gold particles impacting gold substrate. Temperature contour and jetting can be seen in the outer region of the contact area.

In recent studies, it was discussed that adiabatic shear instability may not necessarily be needed to achieve bonding and observing jetting in the contact zones. It was argued that during bonding a large pressure gradient is created in the immediate vicinity of contact surface. The material subject to this pressure acts more like liquid and moves to release this pressure, and jetting occurs similar to a "hydrodynamic spall process." [25]. It should be noted that these studies approach the observation of the bonding phenomena in CS from different perspectives, and the main reason for bonding is a matter of debate.

Figure 2.4 represents a schematic of the jetting process during impact in CS [25]. The first stage shows the formation of shock upon impact of the powder particle and the substrate. The hydrodynamic pressure formed in the first stage is then detached from the leading edge of the particle and the substrate, which can be seen in stage 2. The last stage indicates the occurrence of material jetting due to pressure release from the free surface created in stage 2. The material jetting should reach a threshold value for bonding to occur.
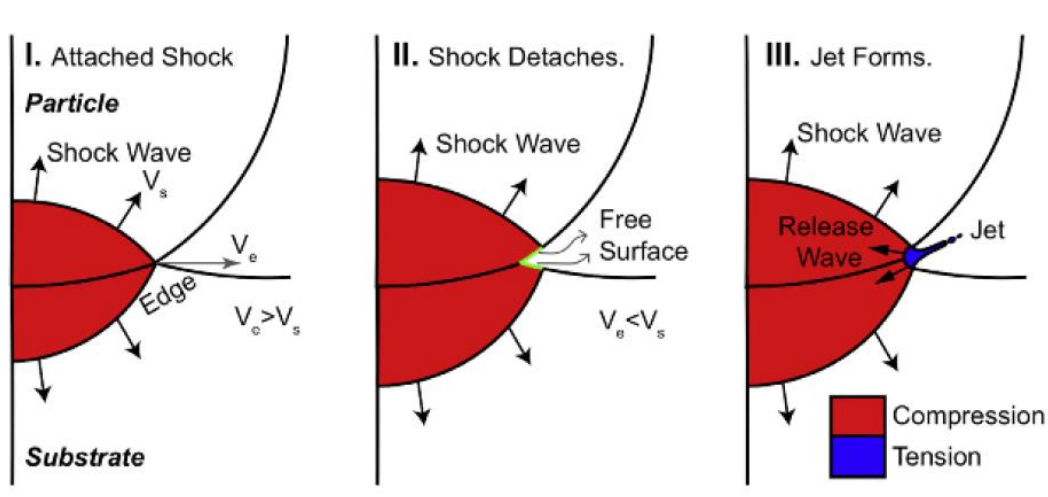
Figure 2.4 Schematic of material jetting in CS. Step 1 represents the shock wave caused by the impact. Stage 2 creation of the free surface caused by shock detach. Stage 3 represents the jet formation due to pressure release [25]

While previous works have proposed different explanations for the occurrence of jetting, they all support the theory that the extreme plastic deformations caused by jetting is the main physical phenomenon that characterizes bonding.

2.3.   Cold Spray Bonding Strength

The mechanical properties of materials are improved within CS applications. This process is done in solid-state, and many studies show the improvement of fatigue strength of materials. As it was mentioned earlier in one the studies of Ghelichi et al [18] it was shown that the fatigue strength can increase by 30% when spraying layers of Al7075 powder on Al5052 specimens. This

study shows the influence of coatings on specimens, and how it increases the strength of the materials. The study points out the coating and substrate bond strength. Similar studies were also done on the strength of the powder deposition and the substrate which resulted in strength increase.

In another study, S.I. Imbriglio [26] utilized CS process and laser-induced projectile impact test (LIPIT) to perform the deposition of Ti powder particles on Al2O3 substrate. The LIPIT is used for real-time observations of particle impact velocity. By using these two techniques they investigated the effect of substrate surface morphology on adhesion strength and particle velocity. It was observed that particles had weaker bonds relative to smoother surface of substrates.

In a study by Rahmati et al [27], metallurgical bonding and mechanical anchoring affected by substrate surface morphology were investigated. The coating adhesion strength was measured for different substrate surfaces. Deposition of pure Aluminum was done on 300M steel substrate. The adhesion strength was around 31 MPa on polished substrates, and significantly decreased to about 6.2 MPa for substrates with low roughness.

In a study by Dina Goldbuam et. al. [28] different deposition condition was applied for spraying high yield strength Ti and Ti6Al4V. The effects of deposition velocity, gas temperature, powder size, and substrate temperature on the adhesion strength were analyzed. Utilizing a micromechanical test technique, the Ti and Ti6Al4V individual splats were sheared to measure their adhesion strength. It was observed that stronger adhesion strength was measured at high velocities (e.g., 1140 m/s) which were much higher than the critical velocity., and preheating the substrate to 400 C. The splat adhesion strength of Ti6Al4V was increased from 100 to 250 MPa with preheating the substrate. The deposition of Ti6Al4V feedstock powder on Ti6Al4V substrate was observed to be not uniform, and the measured adhesion strength was lower than Ti.

The studies point out different important aspects of predicting the adhesion strength in CS process. A full understanding of the CS process and the studies and investigation on this process is yet to be achieved. These previous studies point out the importance of strength in coated materials.

The bonding strength achieved through CS process depends on several factors, such as:

- Particle velocity: Higher particle velocity results in greater kinetic energy upon impact which results in enhance bonding strength.
- Particle material: The material composition of feedstock powder affects the bonding strength. CS is performed with a variety of materials, including metals, ceramics, and polymers. For optimal results, the particle material is compatible with substrate material.
- Particle size and shape: The size and shape of particles influence the bonding strength. In general, smaller particles provide better bonding due to increased contact area and deformation upon impact.
- Surface preparation: Proper surface preparation of the substrate is important for achieving higher bonding strength. The prepared surface should be clean, free from contaminants, and appropriately roughened for better bonding strength.
- Process parameters: Various parameters such as gas temperature, pressure, stand-off distance, nozzle design, affect the bonding strength. Properly optimizing these parameters

for specific material combinations and applications is essential to achieve desired properties.

A direct bonding model was proposed in a previous study in our research group that is capable of predicting the occurrence of bonding [1, 2]. However, this method is not able to predict the bonding strength. In the present research, the direct bonding model proposed in [1, 2] is extended to predict the adhesion strength in case of bonding during the process of pure Aluminum powder sprayed on Aluminum substrate.

2.4. Bonding Strength Prediction

The prediction of adhesion strength, considering the metallurgical bonding in CS is complicated and not straightforward [29]. The bonding mechanism is still being investigated and studied. A number of studies have mentioned that adiabatic shear instability is the mechanism behind metallurgical bonding [24]. Other studies have also discussed and argued that shock wave induced hydrodynamic creates metallurgical bonding [25]. On the other hand, there are studies that consider partial melting caused by localized oxide layer abolition on impact of the particles [22].

Numerical modeling has played a crucial role in investigating the impact of particles on substrates in the cold spray process. Study of the effects of impact velocity and particle diameter [30], material combinations [31], different spray angles [21], to name a few, has captured significant attention in various fields.

Achieving accurate simulations of particle impact has been particularly challenging, especially when using Lagrangian, mesh-based finite element methods. For instance, an FE simulation presented in previous research [24] exhibits Von Mises strain values in the jet region which can reach as high as 400-800%. Such high strains, occurring in a deformation regime dominated by shear forces, can easily cause severe distortion of the simulation elements. Consequently, these high strain values can lead to significant errors in the finite element solution, potentially resulting in the termination of the simulation.

Researchers have employed the Eulerian and Arbitrary Lagrangian Eulerian (ALE) methods. These approaches have proven effective in closely replicating experimental observations. However, the utilization of ALE methods introduces its own set of challenges. For instance, Li et. al. [32] observed unrealistic deformation of particles as speed increases. According to study [33] a comparison of the Lagrangian and ALE methods were made for high-speed impacts. Due to the implementation of mesh morphing in the ALE formulation, it allows us to mitigate the numerical challenges associated with highly distorted elements encountered in the traditional Lagrangian approach. It should be noted that above a certain critical velocity, not only the particle is highly deformed, but also it is embedded in the substrate which is in a flow state. This also creates mesh related challenges in the formulation used in the study.

Meshless methods, namely, Smoothed Particle Hydrodynamics (SPH) have been used to study CS as well. However, it has been indicated that achieving similar results to mesh-based methods

necessitate significantly finer discretization's, specifically a larger number of particles. However, this finer discretization comes at the expense of increased computational costs [34].

Another approach utilized for simulating cold spray is the application of Molecular Dynamics (MD) methods. Particularly, MD simulations have been employed to study microstructural phenomena that take place during particle-substrate impact, including the effects of defect formation, grain boundaries, and structural transformations [35].

The above-mentioned methods will be discussed in detail in Chapter 3. The keynote in these studies is to point out that in most previous studies, the bonding process has not been directly integrated into the numerical simulation. However, in our previous study [1, 2] from our research group the bonding process has been considered and developed within an in-house MPM code (further details will be provided in the next chapters).

On the other hand, in the majority of these studies the calculation of the adhesion strength in bonding scenarios has not been investigated. The goal of this study is to propose a model which complements the direct bonding model proposed in study [1, 2], in order to predict the adhesion strength, while predicting the bonding occurrence.

In the current study the Material Point Method – which will be discussed and investigated in the following chapter – is utilized to firstly investigate the bonding of a single particle impacting the substrate. The bonding model was previously proposed in a previous work [1, 2] and will be discussed in Chapter 4. Second, after investigating the occurrence of bonding in our simulation, the goal of this study which is the prediction of adhesion strength in case of bonding in CS will be investigated and analyzed. The adhesion strength model will be proposed and analyzed in the following Chapter 4. Process parameters and their effects on the model will be introduced and investigated. This work was done following a previous work [1] which proposed the direct bonding model. The current study will utilize the knowledge of the mentioned study to fulfill its goal.

Chapter 3: MPM Modeling of Cold Spray

The major numerical simulation technique often used in solid mechanics applications is the finite element method (FEM) which includes discretizing an object into a finite number of smaller elements with a specific shape, typically triangles or quadrilaterals in 2D and tetrahedra or hexahedra in 3D. These elements form a mesh that approximates the geometry of the object. There are other methods developed based on these concepts that are used for various types of simulations. The important point is how the bodies are discretized and how different methods result in different behavior of the elements. In the following, these methods are first briefly reviewed in this Chapter and their advantages and disadvantages are discussed. The Material Point Method (MPM) used in the present thesis is then discussed in detail and its application to the simulation of particle impact in CS is explained.

3.1. Modeling Techniques

3.1.1. Lagrangian Methods

In the Lagrangian method, it is known that the mesh will deform with the deformation of the material when applying load. A schematic of the mesh deformation in a Lagrangian finite element simulation is shown in Figure 2.4. As the mesh is attached to the material, it deforms with the deformation of the material.
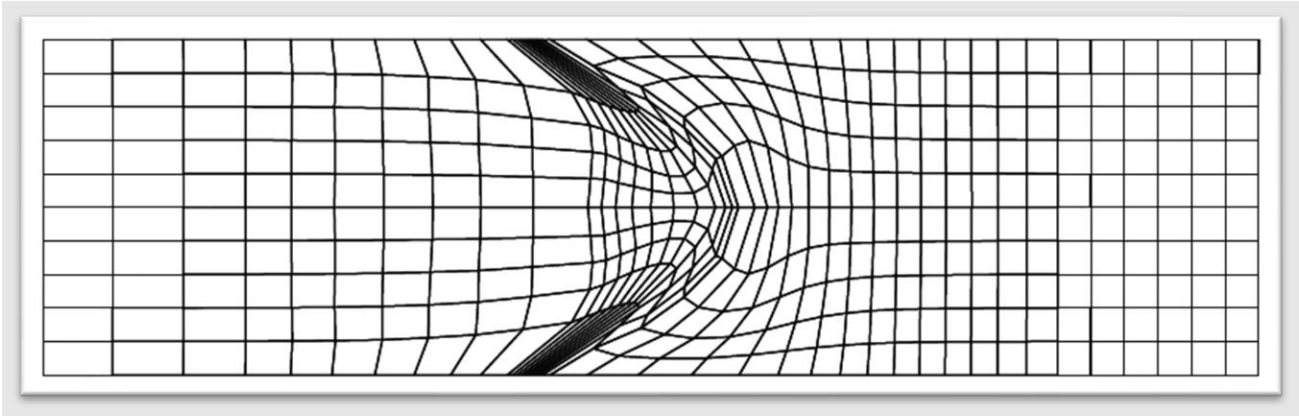
Figure 2.4. Distortion of the mesh alongside with the material in Lagrangian method [36]

Several early studies of the CS impact process were performed using the Lagrangian finite element method. Bae et al. [37] investigated the effect of particle size in coatings, Yin et al. [38] considered the effects of the spray angle, and Hassani et al. [22] studied the effect of oxide layer on adhesion in CS. The material jetting caused by extreme plastic strains and deformations make the investigation and observation of the phenomenon difficult when using traditional mesh-based methods. This issue is caused since the material behaves similar to flowing fluid in contact region

The mesh distortion is an issue when performing simulation with large deformations using the Lagrangian finite element method. The sever distortion in the grids will result in issues such as inaccurate results or pre-mature termination of the simulation due to numerical issues such as negative element Jacobians [36]. In that case, it is deemed more suitable to utilize other approaches and methods. In the case of CS extreme strains and deformation occur and the Lagrangian method is arguably not suitable.

3.1.2. Eulerian Methods

The Eulerian method is typically used in fluid simulations and modeling, but it has been used in solid mechanics as well. The Eulerian method negates the issues of the Lagrangian method concerning mesh distortion. In the Eulerian method while the body deforms the grid will remain in its original position. Figure 2.5 shows a schematic of the results obtained using a Eulerian simulation. As seen, the material moves through the grid. As the grid does not experience any deformation, the issues of mesh distortion can be effectively avoided.
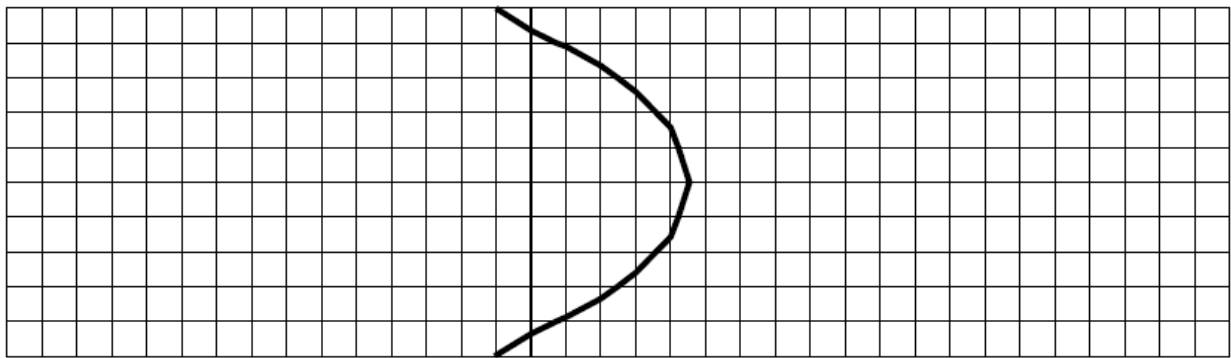
Figure 2.5. Mesh remaining in its original position while the body deforms in Eulerian method [36]

The Eulerian method is capable of modeling large deformations but in the case of our study and also in general, this method has its disadvantages which will be an issue for our study as well. Some of these problems include numerical dissipation of the variables with time, difficulty in enforcing boundary condition in contact problems (like the case of CS), and the high complexity and computational cost of tracking history variables (e.g., effective plastic strains) within the body. In addition, it has been shown that Eulerian methods require significantly finer meshes to achieve similar levels of accuracy as the Lagrangian methods. These challenges lead to increased computational costs and make Eulerian methods less desirable.

3.1.3. Particle-based Methods

The above-mentioned methods and techniques are not ideal standalone and impose limitations when used in study of extreme strains and deformations. Another family of methods is

the particle-based methods which usually combines both the advantages of the Lagrangian method and the Eulerian method. One of the early particle-based methods was the Smoothed Particle Hydrodynamics (SPH). This method discretizes the body into a finite number of particles rather than 3D elements. The discretized particles carry all properties of the body. The SPH method lacks the use of grid in its computations. In Figure 2.6 an example of a wavy fluid simulated using SPH is shown.
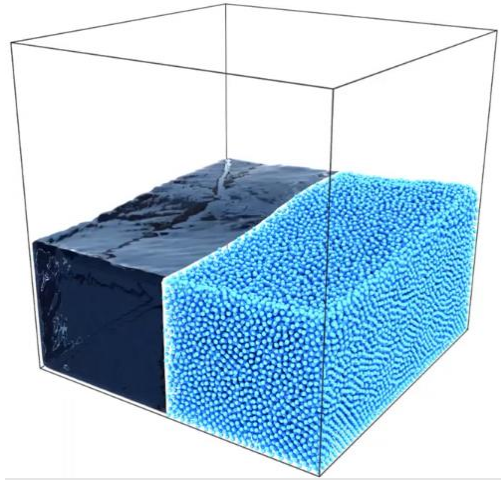
Figure 2.6. Model of a fluid with the use of SPH [39]

The method lacking in mesh will result in particles moving without experiencing mesh distortion which is seen in traditional Lagrangian method.

The use of SPH in CS process modeling has shown good results, but the method is not without disadvantages. Among these issues is the high computational cost of the SPH [36] compared to Lagrangian and Eulerian methods. Furthermore, SPH suffers from the so-called tensile instability issue which implies that particles use physical connection when they are subject to tensile stress. As a result, the simulation becomes unstable so that reliable results cannot be obtained. Even if a solution can be obtained, the tensile instability can lead to over-prediction of the jetting phenomenon [36]. In that case, the particles that fragment away from the main domain due to tensile instability cannot be distinguished from the actual jetting region.

Another meshless method that is proven effective in simulations of CS process is the Material Point Method (MPM) which is the method used in this thesis as mentioned previously. This method is explained in detail in the following.

3.2. Material Point Method

In traditional continuum-based FEM, each body's behavior is described by a series of material-specific constitutive equations following a set of governing equations as well. In MPM

these governing equations are based on conservation law for momentum mass, and energy. The behavior of these equations is similar to those in traditional mesh-based FEM.

In Material Point Method instead of using the total Lagrangian approach, in which the measurements of stress and strain are done with respect to the initial coordinates, the updated Lagrangian approach is used [36]. In the updated Lagrangian approach the measurements are done based on the current configuration using Cauchy stress and rate of deformation. In addition, MPM may be considered as a hybrid Lagrangian-Eulerian method in that each step of the simulation consists of a Lagrangian step and a Eulerian step. The following section will briefly describe MPM.

3.2.1. MPM Overview

The Material Point Method (MPM) [36] is used and implemented in the study of this thesis. MPM is a particle-based method, similar to SPH, in which it incorporates the advantages of both Lagrangian and Eulerian methods. MPM discretizes the bodies into a finite number of material points. Each of these material points carries the stresses, strains, momentum, energy, and all other thermomechanical properties. As it was mentioned earlier the discretization being particles rather than elements will negate the Lagrangian method issue being mesh distortion. Additionally, the constitutive equations will be solved at each material point, and they carry all information, which will result in avoiding the issue of numerical dissipation from the Eulerian method.

The simulations in this thesis were modelled with MPM. It consists of a single particle of a pure Aluminum powder impacting a cylinder (substrate) with the same material. Figure 3.1 represents a 2D schematic of the powder particle before impacting the substrate.

The grid lines represent the computational mesh which discretizes the simulation domain into smaller elements, and the dots represent the body discretization from particle-based method. These material points contain all unknowns such as position, momentum, and other material properties.

The background cells are used for the calculation and interpolation of these unknown values within the material point and are considered to be hexahedron shapes comprising 8 nodes and 6 sides in the 3D analysis. Figure 2.3. shows the shape of the element. As mentioned, these elements serve to interpolate values at each material point by using the element shape functions.
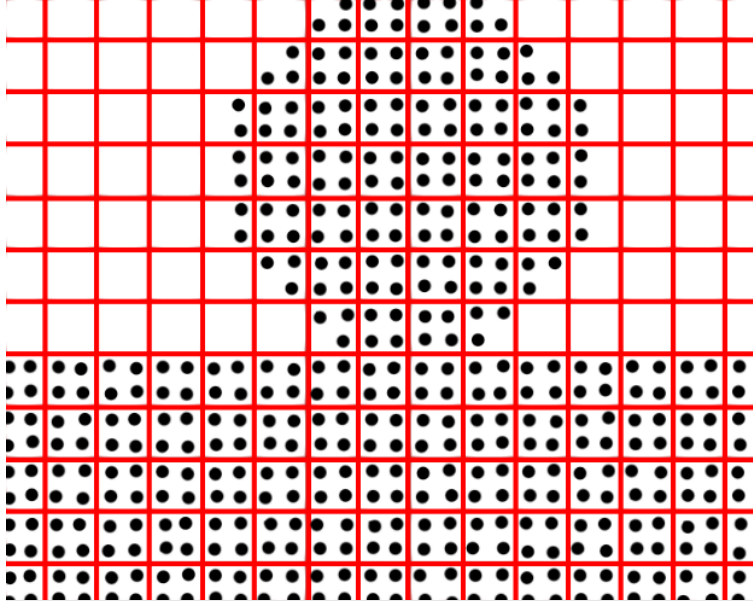
Figure 3.1. Discretization of MPM. the lines represent the background grid, and the dots represent the material

The difference between MPM and SPH is their interpolations in their solutions. SPH is a mesh-less method which utilizes a weighting function known as the SPH kernel. In MPM a computational grid is used and shape functions similar to traditional mesh-based FEM are used.

The MPM is used with an explicit time integration scheme. Different explicit algorithms exist in MPM implementation, including the-Stress-First (USF), Update-Stress-Last (USL), and Modified Update-Stress-Last (MUSL) schemes [27], The MUSL is proven to have better stability properties and is utilized in this work. The overall process in one step of the MUSL algorithm is schematically shown in Figure 3.2. Each explicit step consists of a Lagrangian step and a Eulerian step. Given the stresses, and strains at all particles, the Lagrangian step starts by forming the equilibrium equations at the grid nodes. Note that the material points serve in fact as spatial integration points. The grid is therefore used to integrate the equilibrium equations to obtain the gradient and divergence terms (namely, forces and momentums) at the grid nodes. In fact, the material point data and values will be mapped on their corresponding grid nodes. The nodal velocities and displacements are then obtained by solving the equilibrium equation at the grid nodes. This will give velocities and displacements of the background grid. The Eulerian step then starts by mapping back the velocities and displacements onto the material points. This will update particles displacement, velocity, and momentum. Once the particle positions and velocities are updated, the constitutive equations are solved at each particle to update their stresses, strains, and other history variables. At the end of the process, the grid will be reset back to its original position while the material points remain in their deformed position. This two-step process is repeated at every explicit time step until the simulation is complete. Figure 3.2 [36] represents a schematic for the MPM algorithm.
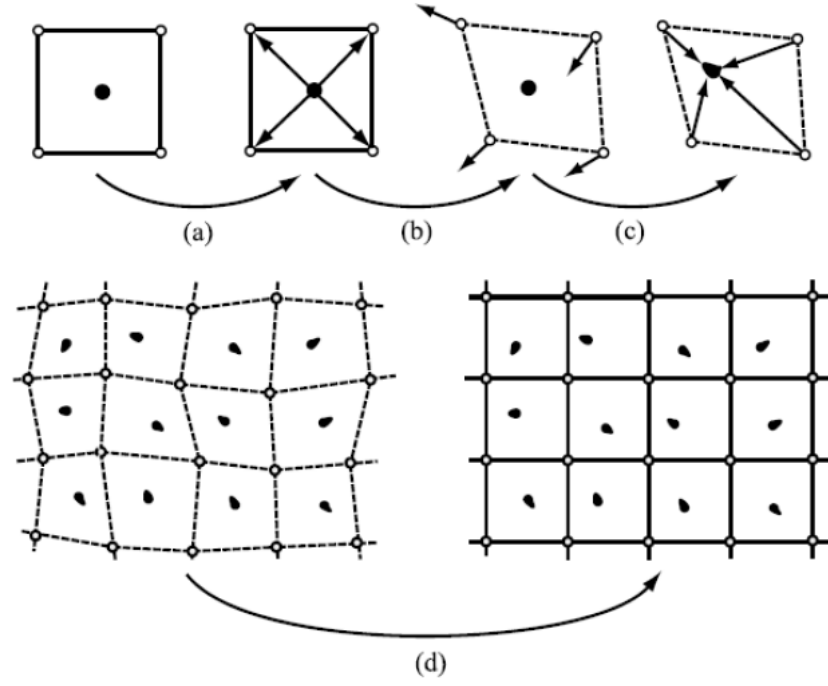
Figure 3.2 Schematic of MPM algorithm. Stage a) material point mass and momentum being mapped on the nodes. Stage b) New nodal forces and momentum being calculated based on material point values. Stage c) updating material point velocity and position with the nodal values Stage d) The reset of background grid and storing material point values [36]

The following section presents formulation and implementation details of the MPM.

3.2.2 Numerical Implementation of MPM

The numerical implementation of MPM was developed by Zhang et al [36]. The present work was done by utilizing the MPM code developed in [36] as a starting point for further implementation of the particle bonding model.

The adhesion strength prediction model presented in this work as well as the direct bonding model proposed in the previous work [1, 2] were numerically implemented within the MPM code. The adhesion strength model and the bonding model will be discussed in Chapter 4. The numerical implementation of the MPM algorithm is presented in the following.

The initial values of mass and momentum are mapped from material points to the computational grid. This process is done through shape functions identical to traditional FEM. The following equations are the mapped mass and momentum. I represents the grid node, p represents the material point and i in momentum represents the direction.

$$m_I = \sum_{p=1}^{n_p} m_p \phi_{Ip} \qquad (3.1)$$

$$(mV)_{iI} = \sum_{p=1}^{n_p} m_p V_{ip} \, \phi_{Ip} \tag{3.2}$$

In the above, n_p is the number of material points in the domain and ϕ_I is the finite element shape function (similar to FEM) associated with grid node I. Furthermore, m_p is the mass of particle p and V_{ip} is the i'th component of the velocity of particle p. The internal and external forces vectors are calculated as,

$$f_I^{int} = -\sum_{p=1}^{n} \nabla\phi_I(x_p)\sigma(x_p)\, v_p \tag{3.3}$$

$$f_I^{ext} = \sum_{p=1}^{n} \phi_I(x_p) b m_p \tag{3.4}$$

where σ contains Cauchy stress values from the previous time step, $\nabla\phi_I$ is the gradient of shape functions at node I, v_p is the volume of particle p, and b is the vector of body forces per unit mass. The discrete equation of motion is used to calculate nodal accelerations based on the internal and external forces at each node as

$$m_I \ddot{x}_I = f_I^{ext} - f_I^{int} \tag{3.5}$$

Equation (3.5) will be integrated explicitly in time. For each time equation (3.5) will be solved for the first phase being the Lagrangian phase, in which the particles are attached to the grid. The Eulerian phase following the Lagrangian phase will reset the grid back into its original position.

With known grid acceleration, the grid momenta can be calculated based on the grid node velocities obtained from the time integration of the nodal accelerations. The grid node momentum values will be calculated and used to detect whether two bodies will come in contact with each other and if contact force is needed or not [1]. The details of contact algorithm are not presented in the present thesis for brevity of presentation. One can find extensive details in [36]. Here, it suffices to say that, in general, contact is detected when the particles of the two bodies are near the same grid node. The present work will predict the adhesion strength of the two bodies in contact in the case of bonding. Details of the model as well as the calculation bonding strength will be discussed Later in Chapter 4.

The simulation continues by updating the material points velocities positions the updated nodal values. The following equation shows the update of each material point velocity and position.

$$V_{ip}^{k+1/2} - V_{ip}^{k-\frac{1}{2}} = \sum_{I=1}^{8} \frac{f_{iI}^k \phi_{Ip}^k}{m_I^k} \Delta t^k \tag{3.6}$$

$$x_{ip}^{k+1/2} - x_{ip}^{k-\frac{1}{2}} = \sum_{I=1}^{8} \frac{\rho_{iI}^{k+\frac{1}{2}} \phi_{Ip}^{k}}{m_I^k} \Delta t^{k+\frac{1}{2}} \tag{3.7}$$

As shown in the RHS summations the number of nodes for each cell containing the material points is 8, namely, a regular grid of 8 noded elements is used. In addition, k represents the time step.

Since the current work utilizes MUSL, the grid node momentums are recalculated from the updated values of material points velocity. These values will then be used to calculate strain and vorticity increments for each material point at each time step.

The strain and vorticity increments will then be used to update the stress of each material point to be used in the next time step. At the end of the time step the Eulerian phase will reset the grid back into its original position. Figure 3.3 shows the MPM algorithm flow chart. This works implementation has been highlighted in the "orange" box.
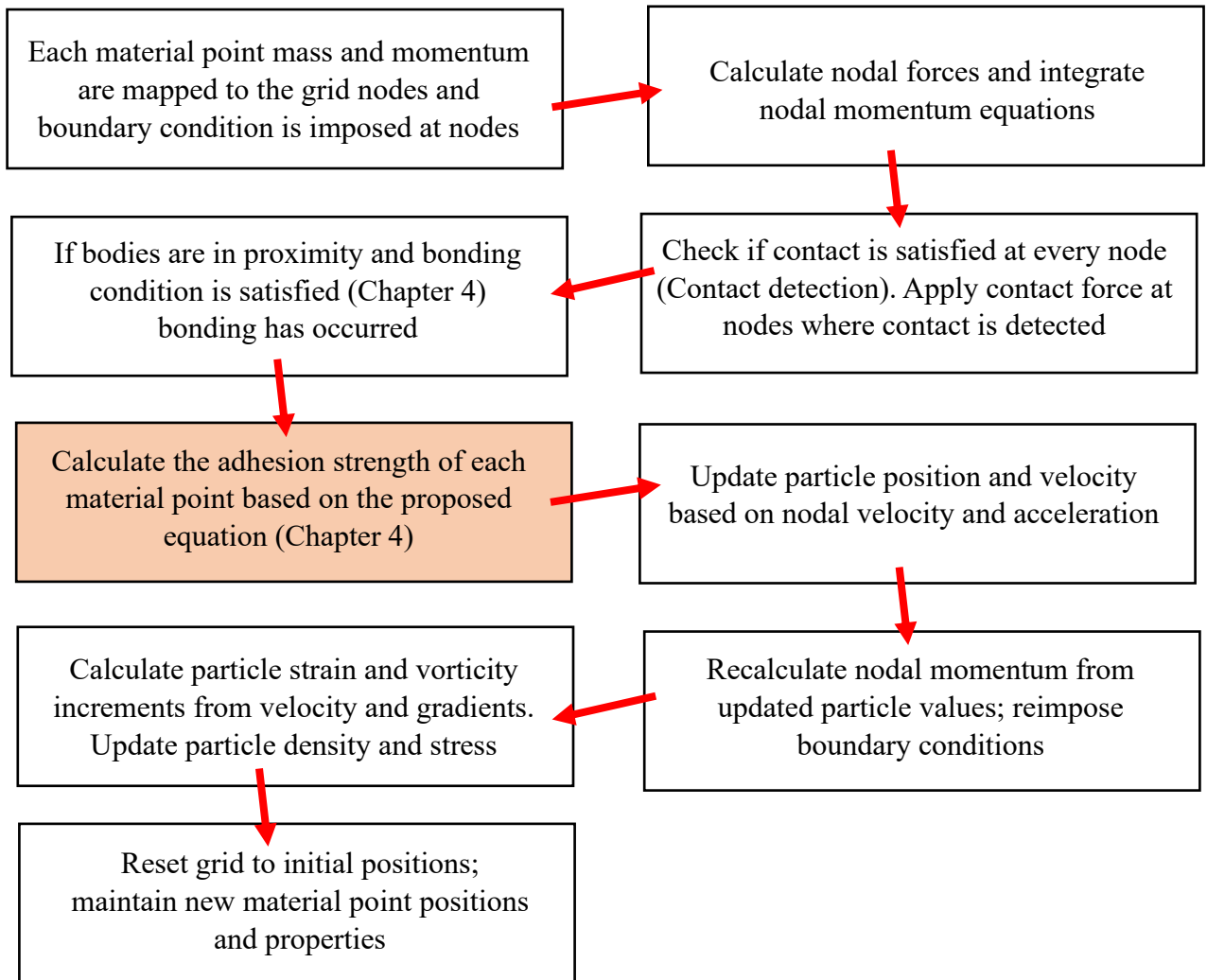
Figure 3.3 Flow chart of MPM algorithm and this works implementation within it

3.2.3   Numerical Considerations

One consideration in this study is the use linear Mie-Gruneisen equation of state as described in Zhang et al [36]. This equation was utilized for determining the internal energy and pressure within each material point.

It should also be noted that adiabatic heating was considered as well. The feedstock material should be at room temperature, but in CS process there is a noticeable temperature change, and it should be considered in numerical modeling [36]. In simulation the output is not relying only on particle temperature. The ratio of the temperature should be between the particle temperature, the reference, and the melting temperature.

Extreme deformation in the jetting region of CS proposes challenges in the normal vector calculation. This is done since the powder particles are traveling at supersonic speeds. The detail of the calculation and the algorithm of the normal vector is discussed in study [1].The current study utilizes this knowledge for its purposes.

Another note that should be highlighted is considering an infinite or semi-infinite media to have a better particle resolution within the particle and decrease the computational cost. The Viscous damping boundary method described by Ross was used to have a finite media act similar to infinite media [36].

3.3   Constitutive Models

In simulations and modeling of microparticles and their impact it is essential to have an accurate description of the material behavior. This is mostly important for conditions such as CS which we are dealing with extreme strains and strain rates and impacts at supersonic speed. The following sections present two of these constitutive models.

3.3.1   Johnson-Cook Strength Model

The Johnson-Cook (JC) [40] model has been used in most constitutive models in CS simulations. On the other hand, the JC model has some downsides at high strain rates.

The JC model might face issues at high strains and also some notes were considered that JC has very small strain rate dependence at high temperatures [41]

All in all, this constative model is not suitable for this study and using this model might cause inaccuracies and issues. The following model is used in this study.

3.3.2.   Preston-Tonks-Wallace Strength Model

The Preston-Tonks-Wallace (PTW) can model plastic deformation with consideration of strain rate and thermal effects. Its development allows it to be used in extreme shock regime. The values of strain rates can be greater than $10^7 s^{-1}$. Previous studies have shown advantages of the PTW model over the JC model in numerical simulation of particle impact in CS.

Due to the benefits of the PTW model on JC model, the current study uses the MPM code by Zhang et al [36] with the addition of PTW strength model in the original MPM code. The flow stress within each material point is calculated with the use of this model [36].

3.3.   Verification of MPM code

Before getting into Chapter 4 and discussing bonding and adhesion strength in CS; the MPM implementation is first verified against existing theoretical solution. To do so, the in-house MPM code was modified and changed to meet the conditions of a classic study of a plane-strain response of a thick hollow cylinder subjected to uniform dynamic pressure [42].

In general, the MPM code functions are based on nine different Fortran90 source files, which function parallel with each other while reading the input file. The present verification allowed the study and investigation of these subroutines in a systematic way and effectively.

The study analyzed and obtained the displacement of the cylinder through its thickness using elastodynamic solution.

Figure 3.4 represents a mesh representing a quarter of the symmetrical cylinder subjected to dynamic pressure (red arrows). The pressure is as follows.

$$P(t) = P_0(1 - e^{-c_0 t})$$

where P_0 and c_0 are constant values of 20 MPa and 10 s^{-1} [42] The inner radius was set to $R_i = 1250 \; mm$ and the outer radius $R_o = 1500 \; mm$.

The cylinder defined in the mentioned application was modeled, and the boundary conditions were applied in the input file of the in-house MPM code The uniform pressure on the inner layer and the conditions for applying the pressure were implemented within the source file. (i.e. "particle.f90" file being one of the source files was modified for the implementation of pressure on the inner layer.)

For the visualization of the cylinder mentioned, which was shown in Figure 3.4, the GMesh software was used. It should be mentioned that GMesh only provides a tool for discretizing bodies and is used here only for visualization purposes. The cylinders' grid cell size was set to $DCell = 3 \; mm$, and the particle spacing was set to $dp = 1.5 mm$.

More important, the results obtained from the in-house MPM code, more specifically, for the visualization of this studies goal being the prediction of the adhesion strength in case on bonding in CS (from Chapter 4 until the end of the thesis) the ParaView software is used.
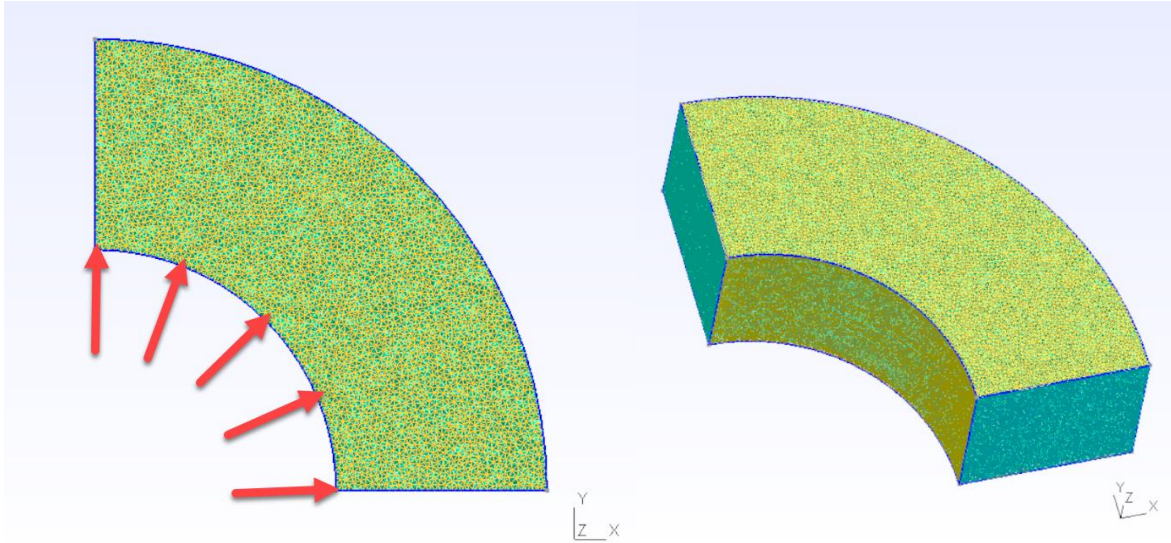
Figure 3.4. Schematic of a quarter of the Cylinder subjected to dynamic pressure. Red arrows represent the pressure

The mentioned equation and the cylinder modeling were done using the MPM code. As shown in Figure 3.4 the quarter of the cylinder was modeled and the dynamic pressure was applied to the cylinder.

Figure 3.5 shows the plot of the results obtained from the MPM code and the mentioned study [42]. It can be seen that the results are reasonably near each other. It should be noted that the root mean square (RMS) calculated for the displacements achieved in study [42] is about 0.1058, and the RMS calculated utilizing the results obtained from in-house MPM code is about 0.1088. These values are reasonably close to each other, indicative of the accuracy of the results obtained numerically using the MPM code.

It should be mentioned that the discretization value and sensitivity influenced the results. Six tests with different discretization levels were performed, and it showed that the smallest discretized value test (which is presented in Figure 3.5) had closest values to the previous study. Also, the overall solution quality remained the same for different discretization considered.

Figure 3.5 Radial displacement through the cylinders thickness. Results compared between MPM study and elastodynamic solution in study [42]

Considering that the discretization level also was a parameter influencing the results, which led to six tests being performed to achieve a reasonably close result to study [42], it should be noted that the computational efficiency of tests performed were also high and the computational cost of performing these tests were reasonable.

Chapter 4: Adhesion Strength Bonding Model

As mentioned earlier, many studies have been done on the effects of process parameters on the adhesion strength, microstructural evolution, mechanical properties, and fracture behavior of materials in CS [43, 44, 45, 46]. These studies point out the importance of the observation of the bonding phenomenon, and how the process of impact is affected by certain parameters. In the following section the bonding model proposed in studies [1, 2] will be discussed.

In section 4.2 the adhesion strength prediction utilizing works [1, 2] will be thoroughly discussed. The affecting process parameters will be mentioned and both observations of numerical and experimental studies on the prediction of adhesion strength will be discussed.

4.1.   Direct Bonding Model

In studies [1, 2] the implementation of the direct bonding model introduces a new history variable known as the bonding parameter (D_{bond}) on the contact boundaries. Its value determines if bonding has occurred in the contact region or not.

In this study we will not get into the details of evolution of the bonding parameter, but in short, the first implementation of the bonding parameter used the surface strain and strain rate to calculate increments of ΔD at each time step [1]. This was further changed into using the surface energy and energy rate to calculate ΔD_{bond}, the increment of bonding parameter at each step. This change was done due to the results of several sensitivity analyses tests [1, 2].

This study utilizes the latter model of the energy-based direct bonding model [1, 2]. The direct bonding model used in this study consists of two material constants, first being the critical adhesion energy G_c, and second the critical adhesion energy rate $\dot{G}_c$.

It should be mentioned that the implementation of the proposed direct bonding model in fact had been tested and analyzed with experimental observations [47]. Figure 4.1 represents the numerical study of the single particle impact of pure Al using MPM and considering the direct bonding model. It can be seen in the case of impact and occurrence of bonding, both numerical and experimental observations are very similar in the material jetting phenomena. The material jetting phenomena can be seen in the numerical result since the grid size and the particle spacing size are very small.

The following section will discuss further the direct bonding model utilizing the adhesion energy rather than using strain.
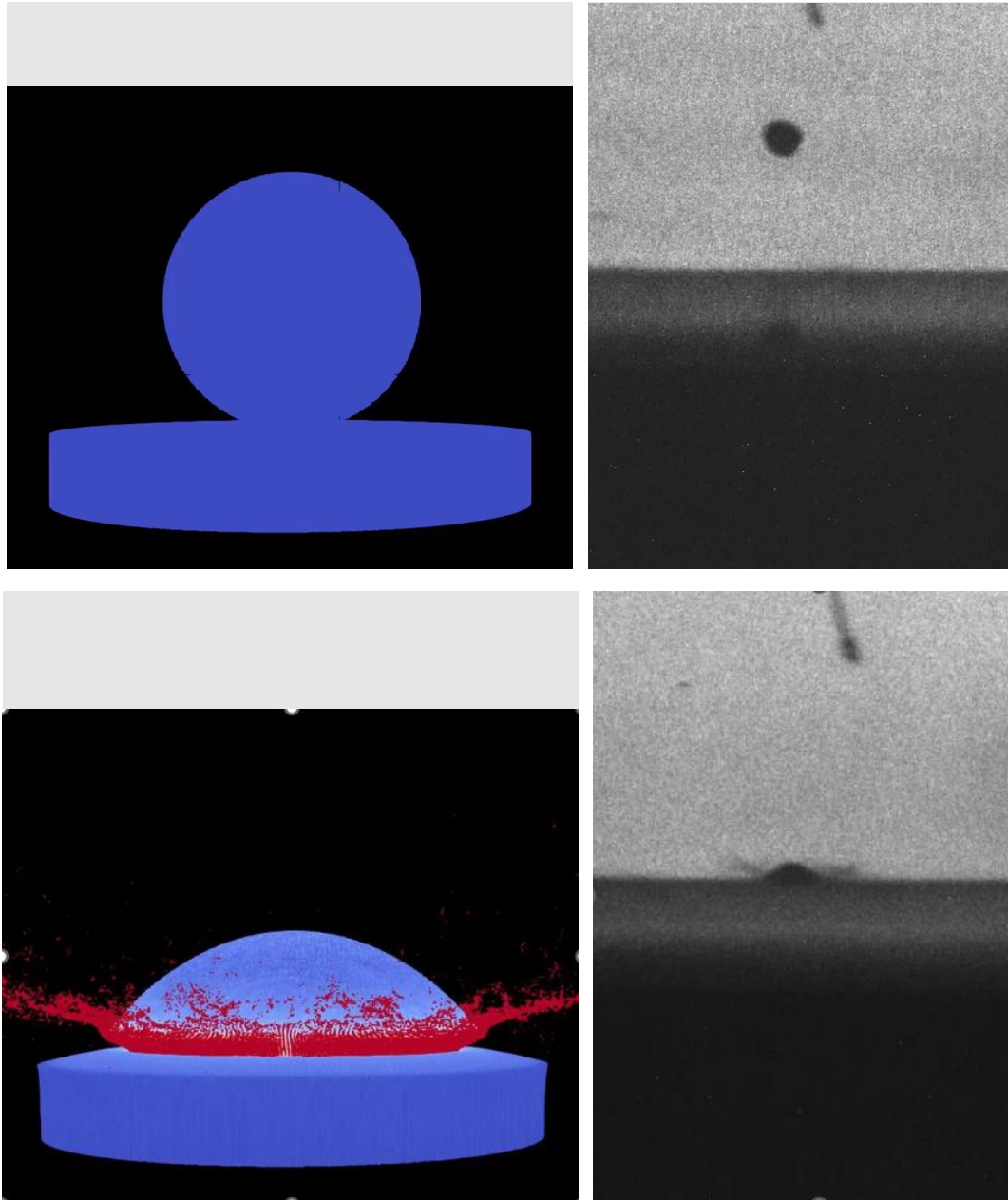
Figure 4.1 The LHS figures represent the numerical study and the RHS figures [47] represent the experimental observations. The top row shows the comparison of both observations before impact. The bottom row shows the comparison of both observations. It can be seen that the material jetting caused by the bonding phenomenon can be observed in both observations

4.1.1. Energy-based Bonding Model

As it was mentioned earlier, the latter model utilizes energy rather than strain to incorporate stress values as well for strength calculations. The bonding parameter (D_{bond}) value determines whether bonding has occurred in the contact region in a specific material point (x_p) or not. Figure

4.1 represents the impact of a single particle, and a brief description of how bonding parameter determines bonding.

The energy-based bonding model is comprised of two material constants. The critical surface adhesion energy G_c, and the critical surface adhesion energy rate $\dot{G}_c$.

The rate of D_{bond} value is considered to be more than zero for material points within the bonding region. Figure 4.2 describes the relation as well. It can be seen that for material points (x_p) in the contact region (S), the value of $\dot{D}$ is more than zero.

$$S = \partial B^1 \cap \partial B^2 \quad \rightarrow \quad \boxed{\dot{D}(x_p) > 0 \text{ for } x_p \in S} \text{ (4.1)}$$
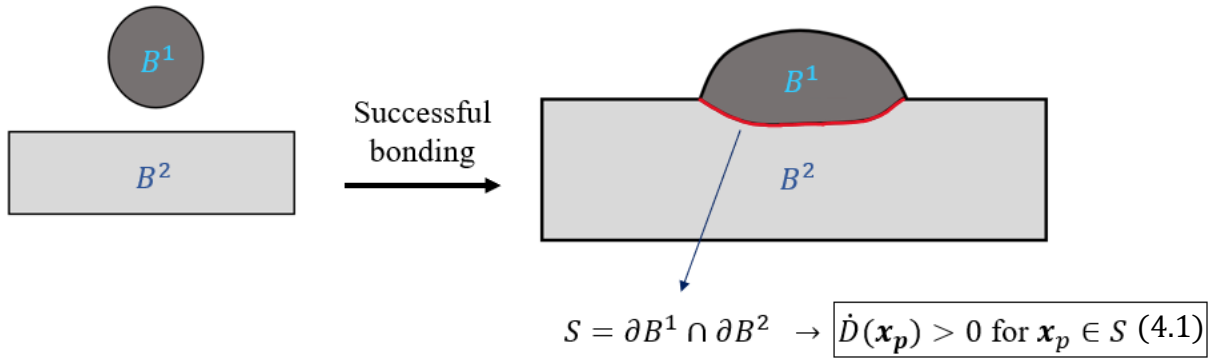
Figure 4.2 Two bodies (B^1 and B^2) are represented. The impact of the particle (B^1) on the substrate (B^2) can be seen in the RHS figure. Considering the red arc being the contact region (S) (In case of occurrence of boning), the $\dot{D}$ value is more than zero for material points in the contact region

The evolution of the bonding parameter for the at each material point on the bonding boundary is as follows.

$$D(x_p) = \sum_{t_1, t_2, \ldots} \Delta D(x_p) \tag{4.2}$$

The $\Delta D(x_p)$ is as follows.

$$\Delta D(x_p) = \frac{\Delta G_s(x_p)}{G_{bond}} \tag{4.3}$$

The G_{bond} in relation (4.4) is dependent on G_c and $\dot{G}_c$. The relation is as follows.

$$G_{bond} = G_c \left(1 - \ln \frac{\Delta G_s(x_p)}{\dot{G}_c \Delta t} \right) \tag{4.4}$$

The $\Delta G_s(x_p)$ represents the increment of the adhesion energy at each material point at each time step. The relation for $\Delta G_s(x_p)$ is also as follows.

$$\Delta G_s(x_p) = \sigma_{vm}(x_p) \cdot \Delta \varepsilon_p(x_p) \tag{4.5}$$

The $\sigma_{vm}(x_p)$ is the von Mises stress and $\Delta \varepsilon_p(x_p)$ is the increment of the effective plastic strain.

It was shown in [2] that the evolution of the bonding parameter is dependent on spatial discretization unless some proper remedies are applied. In this case the bonding parameter increment approaches zero in a limit of mesh refinement. To counter the mesh dependence, a regularization approach similar to what is typically used damage/fracture mechanics is utilized. Recall that bonding may be considered to be a similar but opposite process to damage/ fracture. With this being said, the G_c and $\dot{G}_c$ are replaced by their regularized values.

$$G_c' = \frac{G_c}{h_s}, \quad \dot{G}_c' = \frac{\dot{G}_c}{h_s} \tag{4.6}$$

The new values are obtained by including a measure of the mesh size h_s in the relation. It was shown that [2] with including these regularized values the evolution of the bonding parameter remained consistent with different discretization levels.

4.1.2. Calibration of the Energy-based Bonding Model

Logistic regression was performed in order to determine combinations of critical surface adhesion energy and critical surface adhesion energy rate that leads to bonding of a particle for a given impact velocity. This allows finding a pair of model constants for which the velocity that leads to bonding matches the experimentally measured critical velocities. This set is taken to be the calibrated model constants.

Numerical simulations were conducted in [1, 2] to calibrate the model based on the approach described above. The following notes should be mentioned.

- Two single particle powder sizes were considered (14 micro-meter and 30 micro-meter). Experimental measurements were performed in [21]. The material was pure Al.
- For the 14 micro-meter powder particle, the critical velocity measured is 810 m/s.
- For the 30 micro-meter powder particle, the critical velocity measured was 770 m/s.
- Grid cell and Particle spacing values are 0.7 micro-meter and 0.175 micro-meter respectively.
- 375 different combinations of G_c and $\dot{G}_c$ (375 tests) were considered to obtain the logistic regression plot.

The single splat tests were performed for 99.7% weight Aluminum powder with different combinations of G_c and $\dot{G}_c$. In the logistic regression plot obtained, each combination of the critical surface adhesion energy and energy rate would show whether bonding occurs when the powder is impacting the substrate at its critical velocity.

Figure 4.3 represents the results of the energy-based bonding model calibration. As it can be seen in the two plots (red, representing the 14 micro-meter powder size and blue, representing the 30 micro-meter powder size), the intersection point being Data 1 shows that the combination of G_c and $\dot{G}_c$ for both powder sizes will result in bond initiation.

It should be noted that the combinations of G_c and $\dot{G}_c$ which are below the corresponding plot (bonding/decision boundary) will result in a bonded state whereas the combinations of G_c and $\dot{G}_c$ which are above the plot will result in a non-bonded state.

The intersection point value of G_c and $\dot{G}_c$ obtained from this calibration (Data 1) will later be used to predict the adhesion strength of this test. Other combinations which will result in bonding will also be observed and be studied for the adhesion strength prediction.

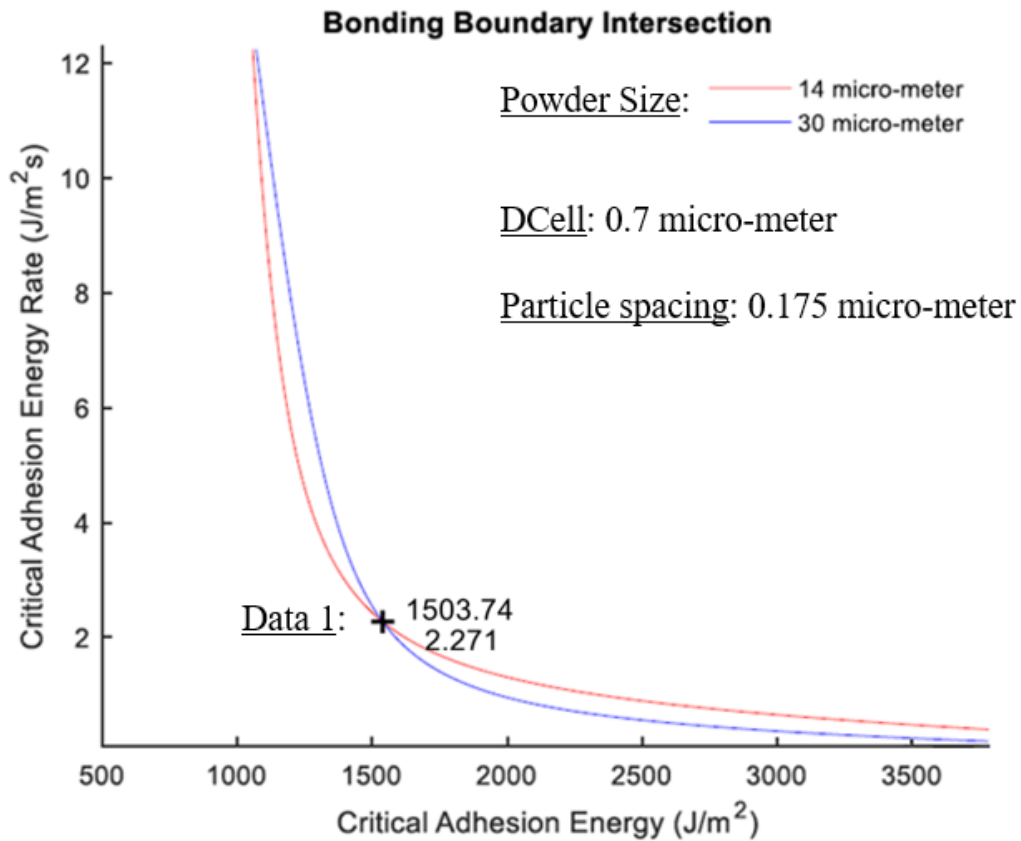*Figure 4.3 Logistic regression plot obtained for two particle powder sizes. 375 tests (different combinations of critical surface adhesion energy and energy rate) were performed to obtain the different combinations and observe whether it results in bonding or not on impact in critical velocity. Combinations below the plot are resulted in bonded and combinations above the plot are considered non-bonded.*

All test results discussed in this study consider the same values of DCell and Particle spacing mentioned earlier and in Figure 4.3. The following section will discuss the adhesion strength prediction.

4.2.   Adhesion Strength Prediction in CS

This section will discuss how the adhesion strength model was proposed and how it utilizes the energy-based bonding model to predict the adhesion strength in occurrence of bonding. In other words, the energy-driven boding model will be enhanced to be capable of predicting the adhesion strength at bonded zones as well

The following sections will discuss adhesion strength calculations and studies from numerical and experimental point of view. The implementation of this study's proposed prediction relation will be shown and discussed.

4.2.1.   Adhesion Strength Prediction (Numerical Aspect)

Most studies on adhesion strength calculations are done through experiments and tests, which require a lot of time for testing numbers of tests to analyze the effect of different process parameters on the adhesion strength of CS process on impact. Utilizing numerical studies will help this issue and will facilitate the number of different tests we can perform.

In a review study [48], different methods of numerical modeling were performed and analyzed. This study modeled particle impact. Deformation mechanism, prediction of critical velocity, and residual stress in areas of interest were studied.

Study [49] utilized Molecular Dynamics (MD) to study the bonding mechanisms and interlockings in copper/copper system. It was suggested that local melting at the interface led to adhesive bonding. It was also discussed that based on their observation the bonding mechanisms was a combination of metallurgical, mechanical and grain boundary interlocking at the interface.

In study [29] a semi-empirical equation was proposed to calculate the adhesion strength as a function of rate of increase of the gradient of the temperature (namely, $\ddot{T} = \frac{d^2 T}{dt^2}$). The study [29] performed numerical modeling as well as experiments. Their numerical modeling was setup in ABAQUS/explicit software. The proposed semi-empirical equation function behavior served as a basis for this study's proposed relation for prediction the adhesion strength. In our case, the empirical evolution function is dependent on the bonding parameter (D_{bond}). The model will be discussed in detail in Section 4.3.

4.2.2.   Experimental aspects in prediction of adhesion strength

As mentioned in the previous section, study [29] observed SEM images of single-particle impact. In different conditions in which the results would be bonded particles, these SEM images consisted of two distinct regions. Figure 4.4 represents a single particle of Ti-6Al-4V impact at velocity of 730 m/s. The first region is a circular shape in the form of an outer ring. This region is where contact was observed. The adhesion strength was also calculated with a strength value. The

second region is the mid-section known as the south pole which its temperature is relatively low, and no bonding was predicted in this region. This will also be observed in the results of this study which the south pole did not predict any adhesion strength.
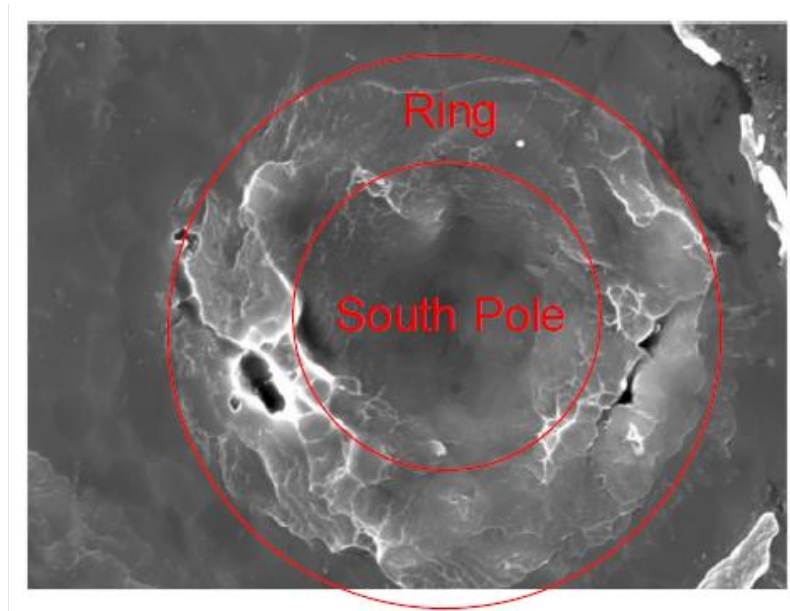
Figure 4.4 Bonding region for a single particle of Ti-6Al-4V impact at 730 m/s. The SEM image shows that 60% of the contact area is bonded [29].

Study [50] also observed similar results. As it can be seen in Figure 4.5, the south pole (red box) is observed to be the nonbonded region while the ring (green box) is the bonded region.
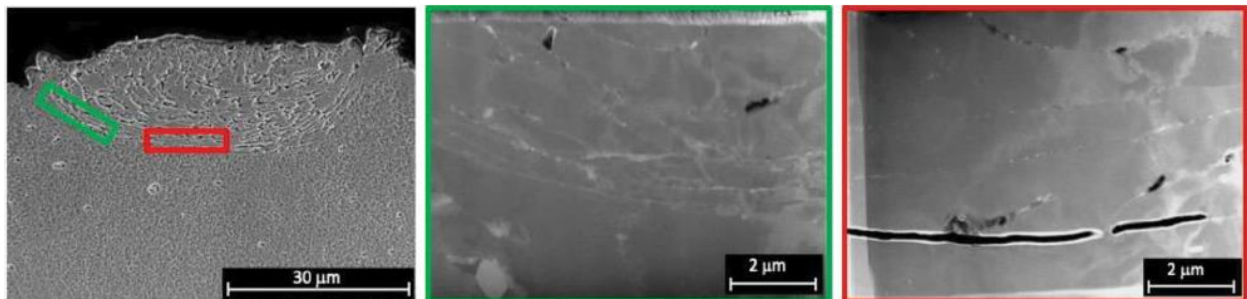
Figure 4.5 Bonding region of Al-6061 deposition. The bonded and nonbonded areas can be seen in the green and red box respectively [50]

Study [44] considered factors affecting the bond strength of Al powders in CS. The study focused on studying other materials in CS such as ceramics for substrate. The influence of substrate material, substate temperature, and particle size were investigated. Another study [51] investigated the effect of coating thickness on the adhesion strength and residual strength. A powder formed on

the chemical composition of IN 718 was sprayed on IN 718 substate. It was observed that the adhesion strength of coated areas would decrease with the increase of coating thickness.

4.3. Adhesion Strength Numerical Implementation

As it was mentioned earlier with observing and investigating the sigmoid behavior of the semi-empirical equation [29] this study proposes the following relation (4.7) for the prediction of the adhesion strength. This relation complements the current energy-based model proposed in study [1, 2]. The adhesion strength evolves based on the following relation.

$$\sigma = \sigma_c \frac{1}{1 + e^{-K(D_{bond} - \kappa)}} \tag{4.7}$$

In the above equation σ represents the bonding strength predicted at a material point. The material constants, σ_c is the maximum bonding strength achievable at a material point. D_{bond} represents the bonding parameter proposed in study [1, 2]. κ is the threshold for D_{bond} at which the adhesion strength build-up triggers. K is the tuning parameter and shows how quickly the adhesion strength builds up at a material point. (Namely, the rate at which the function goes from 0 to σ_c).

Figure 4.5 represents the sigmoid behavior of adhesion strength function σ in relation to the bonding parameter D_{bond}. The change of the function's builds up with the change of the tuning parameter (K) value is also shown in figure 4.5. It should be noted that the value of the input of this relation which is the bonding parameter (D_{bond}) will not achieve the high values presented in figure 4.5. Most of the observations from the simulations showed that the values remained under 10.
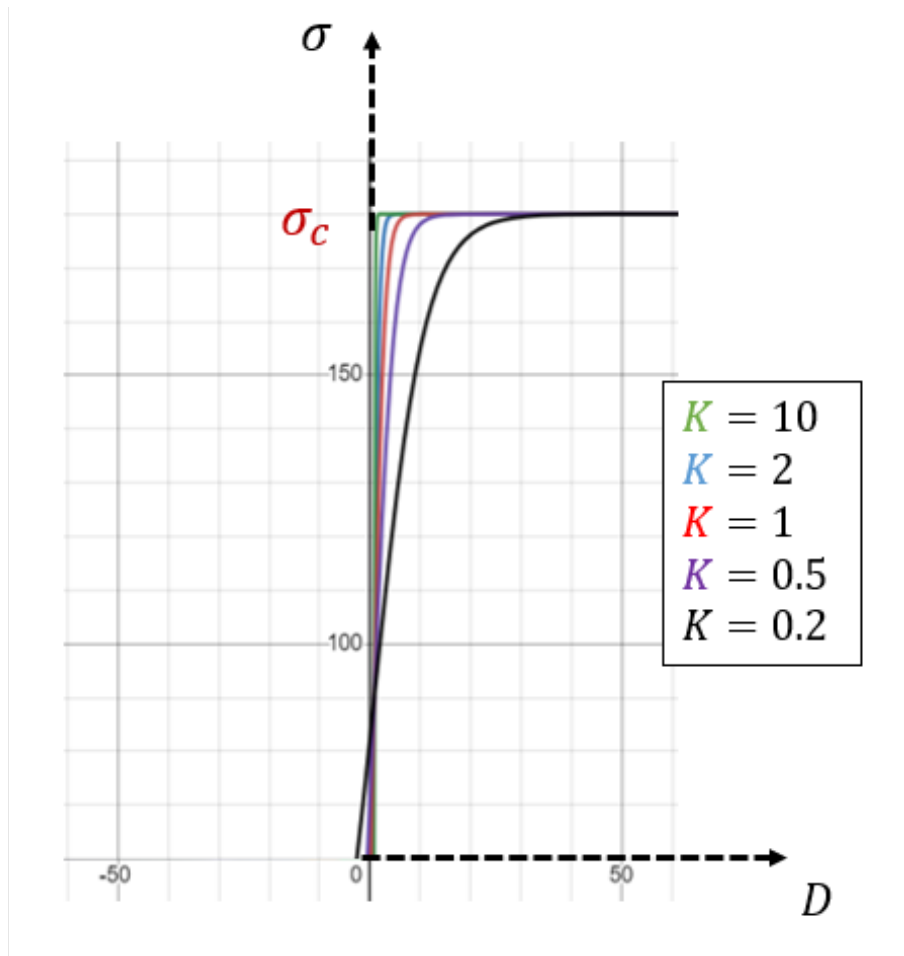
Figure 4.5 Adhesion strength model prediction output (σ) in relation to the bonding parameter (D_{bond}) [1, 2]. Change of adhesion strength build up with the change of the tuning parameter (K)

The implementation of this relation is done in the method mentioned in Chapter 3 which was MPM. This method consists of two phases in each time step. The first phase being the Lagrangian phase in which the particles are attached to the grid. The velocity and the position are updated based on solutions achieved from equation 3.5 in Chapter 3. The second phase, being the Eulerian phase, will reset the grid back to its original position while the material points remain in their updated form. The information stored in the material points will be mapped onto the new grid nodes of the next time step. This will allow the initiation of the solution for the next time step. The stresses are updated within each time step with the use of the Modified Update Stress Last (MUSL) scheme.

The bonding and the prediction of the adhesion strength is included with assigning each material point in the boundary surface of the particle-substrate model with one bonding parameter (D_{bond}) and one adhesion strength parameter (σ). The particles' bonding parameter is mapped to the grid nodes similar to other information such as velocity and acceleration.

Chapter 5: Numerical Results and Discussion

This chapter will discuss the results obtained from the implementation of the adhesion strength prediction method presented in the previous Chapter. This chapter is discussed in two sections. The first section will discuss the relation implemented in the MPM code and the values defined for the parameters will also be presented. The predicted adhesion strength distribution and the values obtained will be shown. The average adhesion strength obtained from the impact is also presented. The second section will discuss the sensitivity of the presented relation in this study for predicting the adhesion strength in relation to G_c and $\dot{G}_c$ and will show how the change in these values (considering that the combination maintains in the bonding region discussed in Chapter 4) will affect the predicted adhesion strength and the distribution achieved on impact.

Before discussing the results obtained from the simulations, some key notes are presented and should be considered.

The simulations in this study were performed considering that the single powder particle and the substrate are both from 99.7% pure Al. For achieving Figure 4.3 both diameters of 14 and 30 micro-meter were considered for the single powder particle but considering that the aim of this study is to predict the adhesion strength in occurrence of bonding (combinations of G_c and $\dot{G}_c$ in bonding region) the results shown in this chapter are for the 14 micro-meter diameter. Therefore, the critical impact velocity is also considered to be 810 m/s.

The presented results, considering the adhesion strength prediction relation (presented in relation 1) consider two trials values for the parameters of the bonding strength model equation (4.7). Note that to obtain the true calibrated value of σ_c for a specific material several experimental tests should be performed. Similarly, for obtaining the exact value of κ the model needs to be calibrated against experimental data. Designing and conducting such experiments are beyond the scope of this thesis. Thus, trial values were assumed for the model parameters as σ_c =180 MPa and $\kappa = 0.85$. This assumption will be discussed in Chapter 6.

5.1. Adhesion Strength Prediction Results

The presented result for this section is considering the calibrated value for G_c and $\dot{G}_c$ achieved from the 375 tests presented in Chapter 4. The results previously shown in Figure 4.3 are repeated again in Figure 5.1 for easier reference. The calibrated combination of the mentioned parameters can be seen in the intersection point of the two curves obtained for the two particle diameters. The calibrated $\dot{G}_c$ and G_c values obtained are 2.271 $J/m^2 s$ and 1503.74 J/m^2, respectively.
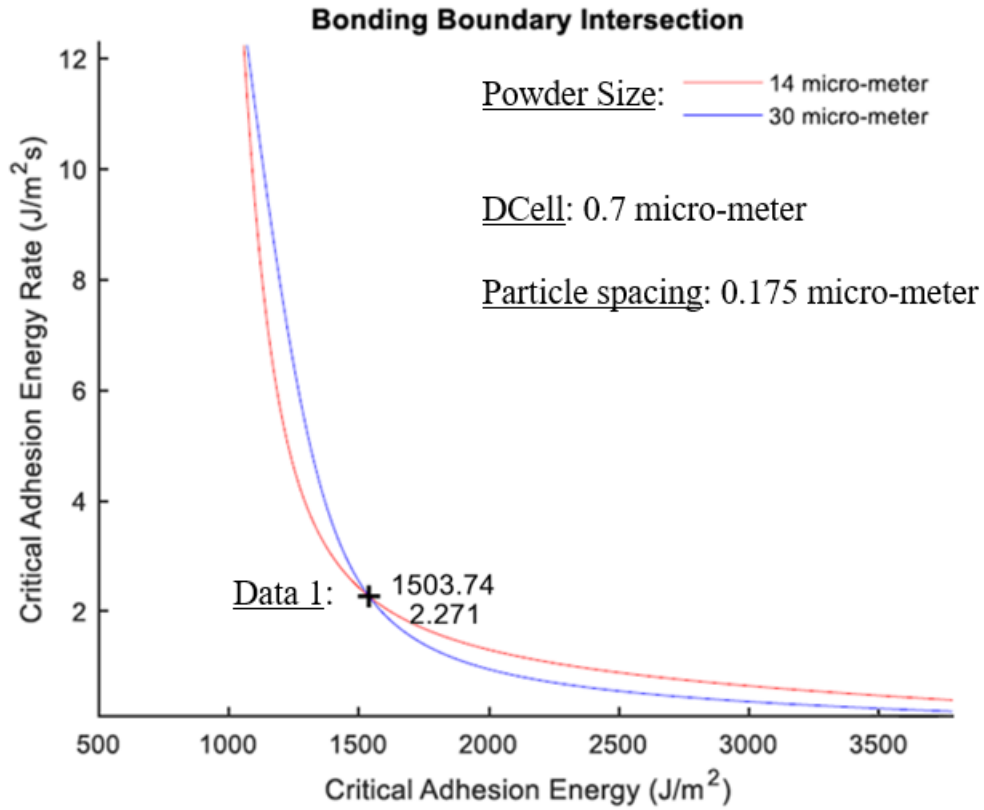
Figure 5.1 Logistic Regression plot discussed in Figure 4.3

Consider the adhesion strength prediction model of equation (5.1) (which is the same equation as the previously presented equation (4.7)). This equation is used to predict the adhesion strength when bonding occurs due to particle impact. Thus, a combination of G_c and $\dot{G}_c$ close and below to the bonding boundary of the particles is considered. The calibrated values of G_c and $\dot{G}_c$ on the calibration plot are not used since for those values bonding has just barely happened and so can cause issues in the numerical simulation. The combination considered for $\dot{G}_c$ and G_c, considering that it should also maintain in the bonding region as well as close to the contact point, is 2.00 $J/m^2 s$ and $1500\ J/m^2$. This combination will ensure the bonding occurrence and also the results achieved were promising considering the combination being near the calibrated point. It should be noted that several other combinations have also been tested and will be discussed further into this chapter.

Recall that the bonding strength mode is given by

$$\sigma = \sigma_c \frac{1}{1 + e^{-K(D-\kappa)}} \tag{5.1}$$

The assumed values of the parameters in relation (5.1) are $\sigma_c = 180$ MPa and $\kappa = 0.85$ as mentioned previously. Furthermore, the tuning value K is considered to be 1 since the rate seemed

to be more effective in comparison to other values. The bonding parameter D_{bond} is known as the input. As it was discussed in Chapter 4, the value of D_{bond} achieved for each material point will show whether bonding has occurred or not. The bonding strength model only applies to material points at which bonding is achieved.

The following section will show and discuss the predicted adhesion strength considering the mentioned values and parameters.

5.1.1. Adhesion Strength Distribution

Figure 5.2 shows the predicted adhesion strength obtained using $\dot{G}_c = 2.00 \, J/m^2 s$ and $G_c = 1500 \, J/m^2$. Results shown correspond to $t = 5 \, ms$ after impact. As can be seen, the adhesion strength is predicted on the outer layer of material points representing the particle's surface. Figure 5.3 shows a detailed view of the distribution of the predicted adhesion strengths shown in Figure 5.2. Note that the adhesion strength is only meaningful for particles that are predicted to be bonding by the bonding prediction model (see Section 5.2). Therefore, material points that are not bonded are excluded from both Figures 5.2 and 5.3. Recall that the bonded particles have a value of bonding parameter greater than 1.
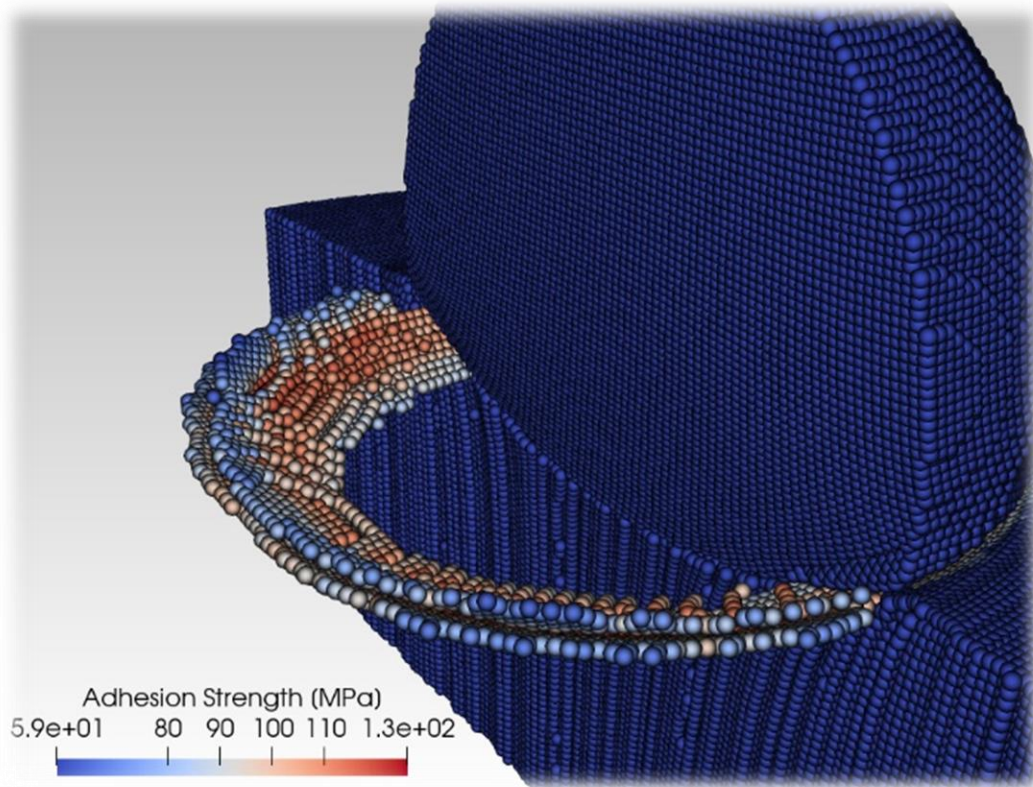

Figure 5.2 The predicted adhesion strength distribution of the impact of a 14 micro-meter Al powder on an Al substrate at 810 m/s. The G_c and $\dot{G}_c$ considered were 2.00 J/m²s and 1500 J/m² respectively. The adhesion strength distribution results vary from 59 to 130 MPa. The average adhesion strength is 42.16 MPa.
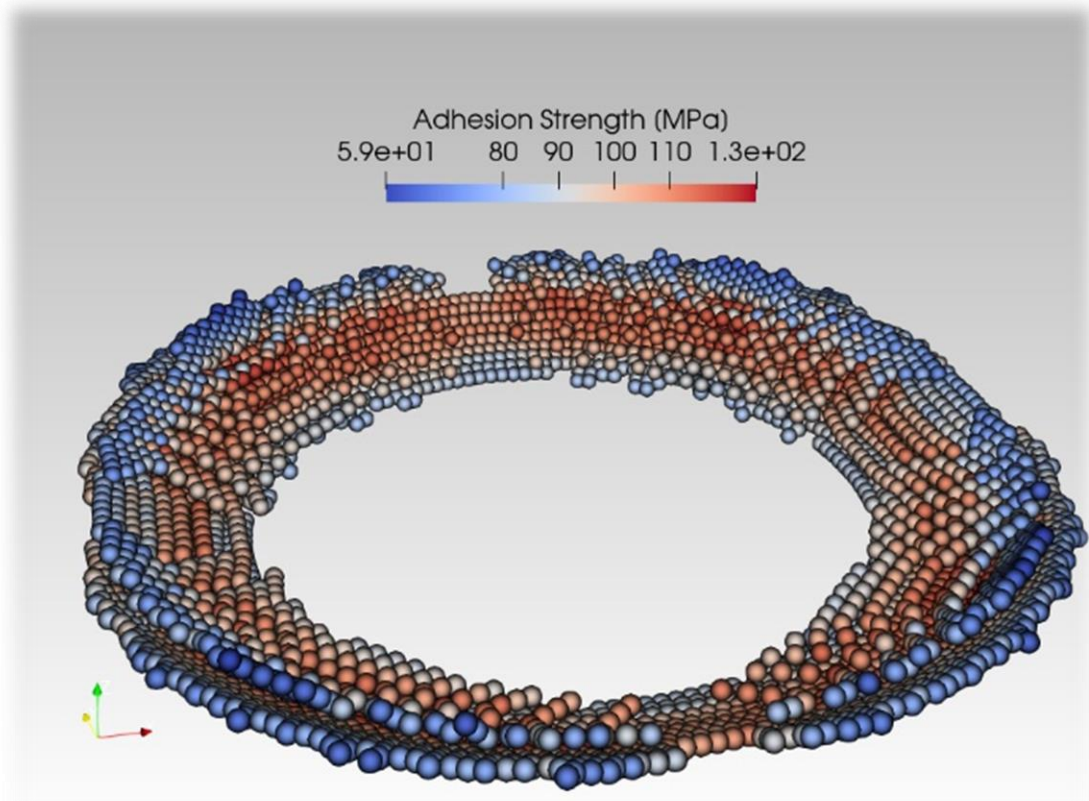
Figure 5.3 The predicted adhesion strength distribution in detail. (The result is figure 5.1 in detail)

As seen in both Figures 5.2 and Figure 5.3, the predicted adhesion strength values for each material point in presented. In a qualitative comparison with the experimental observations shown in Figure 4.4, it can be seen that in the south pole no value for the adhesion strength was predicted which shows that no bonding has occurred in that region. The outer layer which adhesion strength was predicted reaches about the leading edge of the particle and substrate which material jetting occurs in bonding. The predicted values for the predicted adhesion strength in this case varied from 59 to 130 MPa in the contact region.

The following section will discuss the average adhesion strength calculation of the results obtained and will discuss the achieved value for the above conditions. The other values in other conditions considered in the sensitivity analysis section are presented in the same section)

5.1.2. Average Adhesion Strength

The calculation of the average adhesion strength was also implemented in the MPM code. The calculation considers the sum of all bonded material points' adhesion strength multiplied by their mass, all divided by the sum of all bonded material points masses. The calculation was done

parallel to defining the bonded material points. A brief calculation of the adhesion strength can be seen below.

$$\sigma_{avg} = \frac{\sum_{i=1}^{n(bonded)}(\sigma_i * m_i)}{\sum_{i=1}^{n(bonded)} m_i}$$

Considering the condition of the result obtained in section 5.1.1, the predicted average adhesion strength was calculated 42.16 MPa.

Considering study [27] which calculated the adhesion strength to be 31 MPa the calculated adhesion strength from the proposed relation is very promising considering that trials values are used for σ_c and κ, and the combination of the parameter being near the calibrated G_c and $\dot{G}_c$ values

The following section will discuss the sensitivity analysis of the prediction model.

5.2.   Sensitivity Analysis

The purpose of this section is to analyze and study the effect of different combinations of G_c and $\dot{G}_c$ on the predicted adhesion strength on impact. To do so, each of the parameters were kept fixed while varying the other one to isolate its impact on the simulation results. It was made sure that all combinations considered lead to results that remained in the bonded region.

Figure 5.4 shows the calibration plot along with the combinations of model parameters used in the sensitivity analysis marked as red points. Note that the chosen combinations are in the bonded region. The values for both the critical adhesion energy and the critical adhesion energy rate vary between 1000 to 1750 and 0.5 to 5.4 respectively. Table 5.1 summarizes the combinations chosen for G_c and $\dot{G}_c$ taken from Figure 5.4. In the following, results obtained using the above-mentioned combinations of model parameters will be discussed.
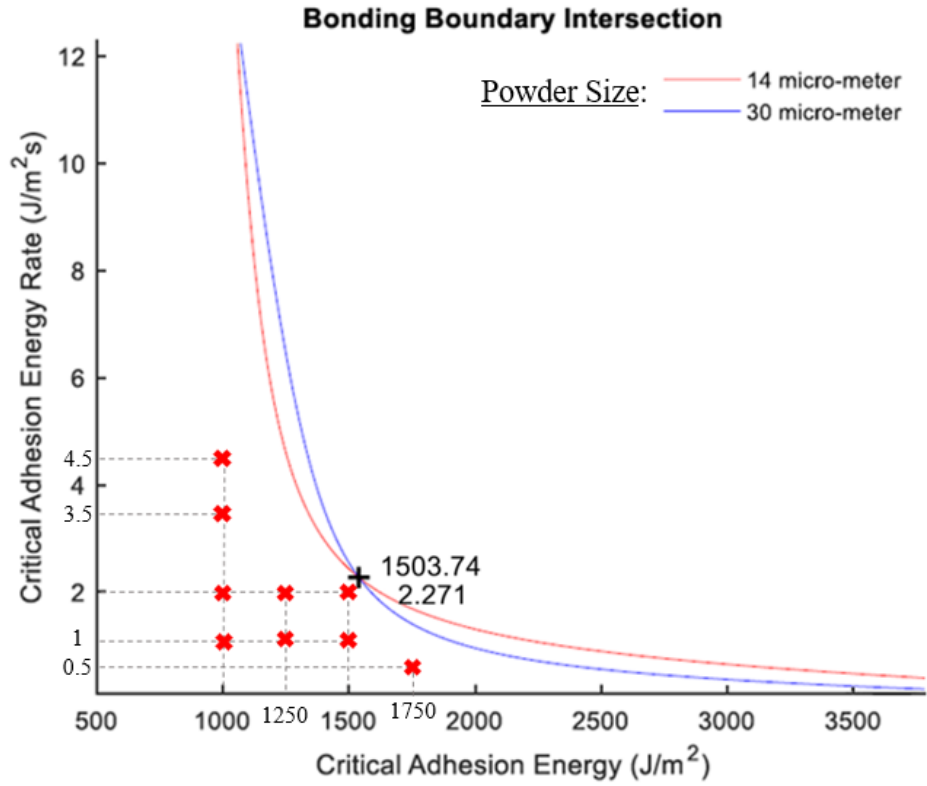
Figure 5.4 Logistic regression plot of critical adhesion energy rate and critical adhesion energy. Red point are combinations of G_c and $\dot{G}_c$ in the bonded region The nearest red point to the calibrated value is 1500 and 2 respectively. The result of this combination was discussed in the previous section.

Gc rate (J/m^2s)	Gc (J/m^2)
0.5	1750
1	1000
1	1250
1	1500
2	1000
2	1250
2	1500
3.5	1000
4.5	1000

Table 5.1 The combinations of G_c and $\dot{G}_c$ which were considered as red points in figure 5.3

41

Figure 5.5 and Figure 5.6 show the results obtained for using $\dot{G}_c = 0.5$ and $G_c = 1750$. The parameters mentioned are the first row of table 5.1. It can be seen that little to no regions of non-bonded area were obtained. The average adhesion strength was about 132.9 MPa, which is very high for CS process and the range of the experimental results do not reach this value. In this case, the adhesion strength values varied from 54 MPa to 180 MPa in contact region.
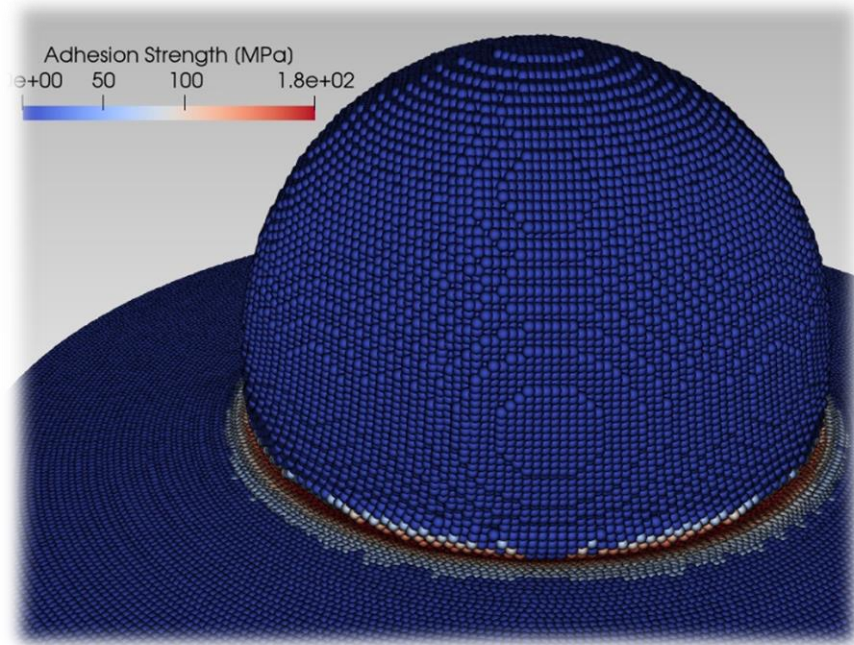

Figure 5.5 Impact of an Al single powder particle onto Al substrate. Combination of G_c and $\dot{G}_c$ being 1750 J/m^2 and 0.5 J/m^2s respectively
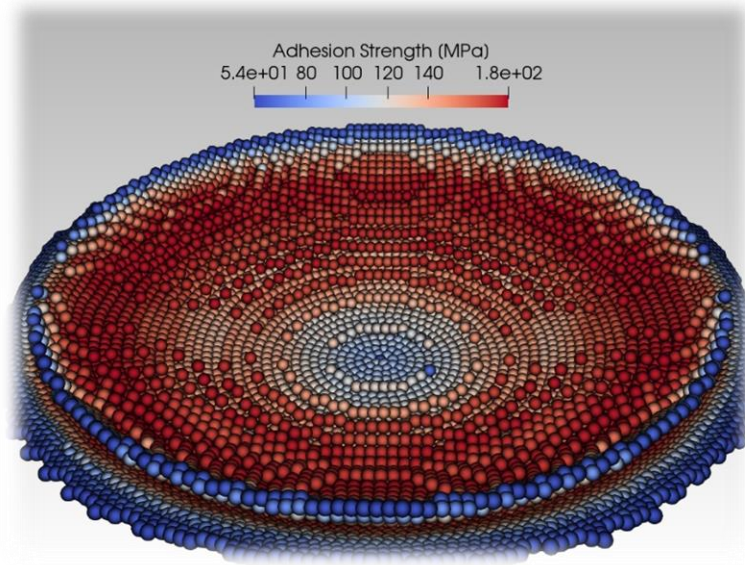
Figure 5.6 Distribution of adhesion strength (Figure 5.4 contact region)

Next, the combination on the second, third, and forth rows of table 5.1 are considered and tested. Figure 5.7, 5.8, and 5.9 represent the results obtained for $\dot{G}_c = 1$ with different values of $G_c = 1000$, 1250, and 1500. From these results, the non-bonded region is observed in the south pole but the results are different for each case. The key conclusion obtained from these tests is the fact that the changes in G_c had little effect on the adhesion strength values. The change is also little in the obsereved contact region and distribution of adhesion strengths.
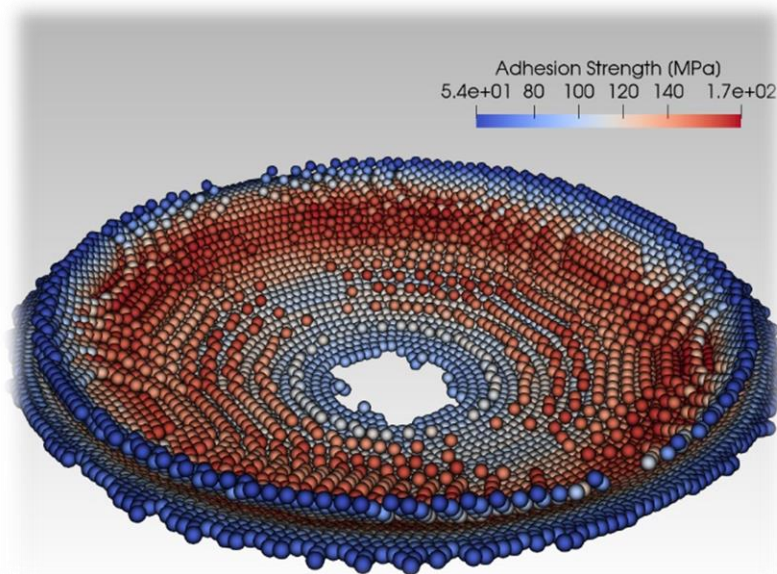

Figure 5.7 Distribution of adhesion strength in contact region. Combination of G_c and $\dot{G}_c$ being 1000 J/m² and 1 J/m²s respectively

Figure 5.8 Distribution of adhesion strength in contact region. Combination of G_c and $\dot{G}_c$ being 1250 J/m^2 and 1 J/m^2s respectively

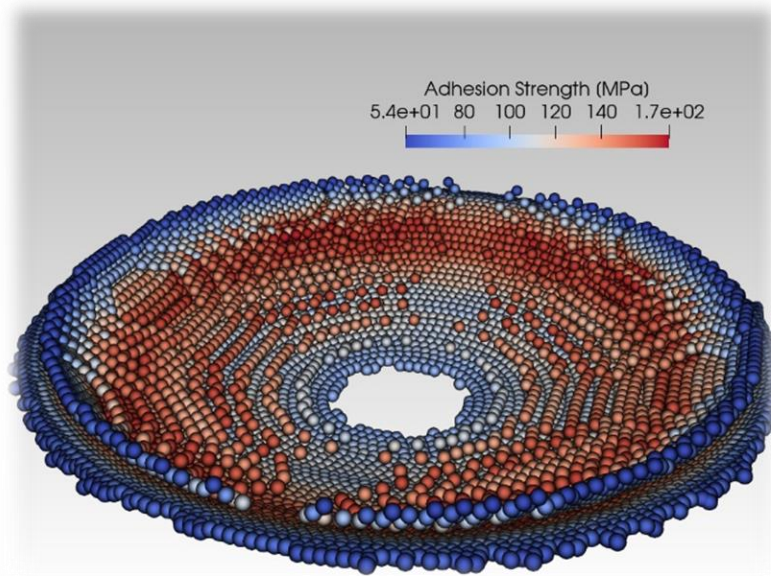*Figure 5.9 Distribution of adhesion strength in contact region. Combination of G_c and $\dot{G}_c$ being 1500 J/m^2 and 1 J/m^2s respectively*

The average adhesion strength achieved for the above 3 combinations were also 107.6 MPa, 103.3 MPa, and 99.86 MPa, respectively. The change of adhesion strength is little with the change of G_c. On the other hand, comparing the results shown in 5.7, 5.8 and 5.9 with the results shown in Figure 5.6 indicates the prediction of the model changes drastically so that a non-bonded area can emerges

in the results when $\dot{G}_c$ increases from 0.5 to 1. For this set of model parameters combinations, the adhesion strength values varied from 54 MPa to 170 MPa on the bonded surface.

Figures 5.10, 5.11, and 5.12 represent the results obtained with $\dot{G}_c = 2$ and different values of $G_c = 1000, 1250,$ and 1500. These correspond to the 5th, 6th, and 7th row of table 5.1. Note that the combination $\dot{G}_c = 2$ and $G_c = 1500$ was also discussed in the previous section. This combination was considered to be a close point to the calibrated $\dot{G}_c$ and G_c values. It can be seen that the non-bonded area has begun to expand with the increase of $\dot{G}_c$, and little changes can be seen with the changes of G_c.

Figure 5.10 Distribution of adhesion strength in contact region. Combination of G_c and $\dot{G}_c$ being 1000 J/m² and 2 J/m²s respectively
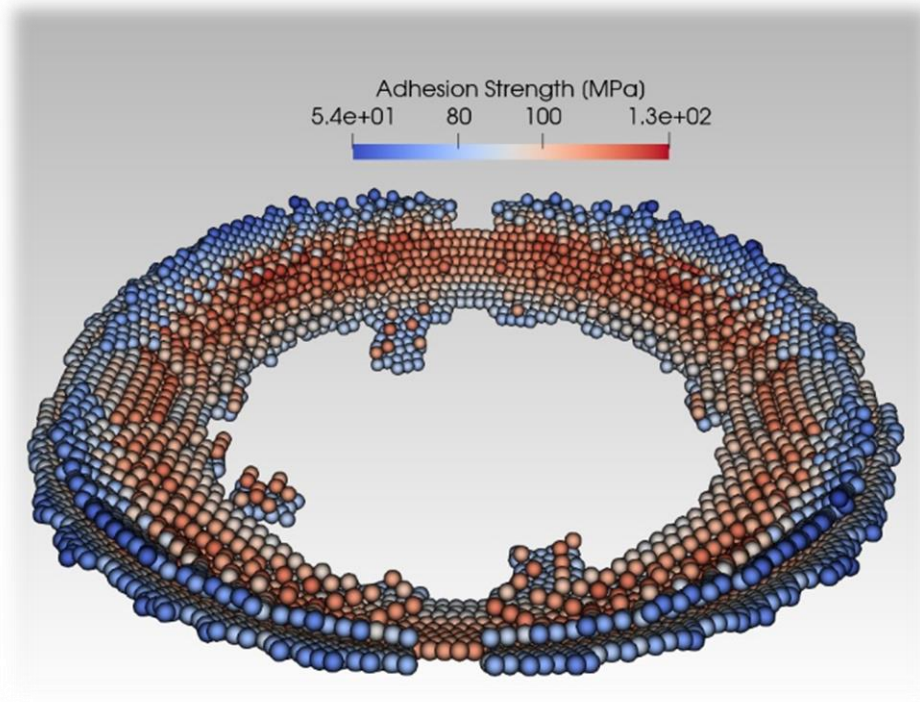
Figure 5.11 Distribution of adhesion strength in contact region. Combination of G_c and $\dot{G}_c$ being 1250 J/m^2 and 2 $J/m^2 s$ respectively

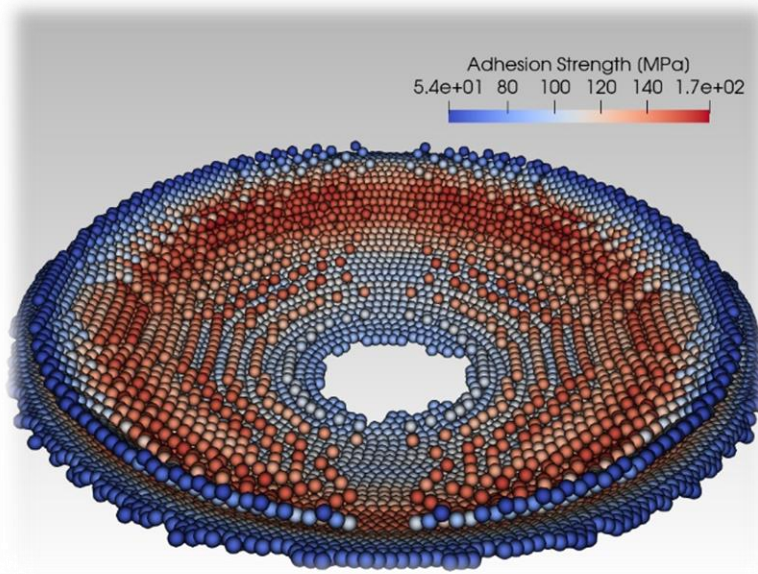*Figure 5.12 Distribution of adhesion strength in contact region. Combination of G_c and $\dot{G}_c$ being 1500 J/m^2 and 2 $J/m^2 s$ respectively*

The average adhesion strength calculated for these 3 sets of tests was 66.39 MPa, 50. 15 MPa, and 42.16 MPa, respectively. The non-bonded area has increased in comparison to $\dot{G}_c = 1$.

Figure 5.13 shows the results obtained with $\dot{G}_c = 3.5$ and $G_c = 1000$. It can be seen that the non-bonded region is growing with the increase of $\dot{G}_c$. Also the averge adhesion strength achieved was 36.47 MPa for this condition.

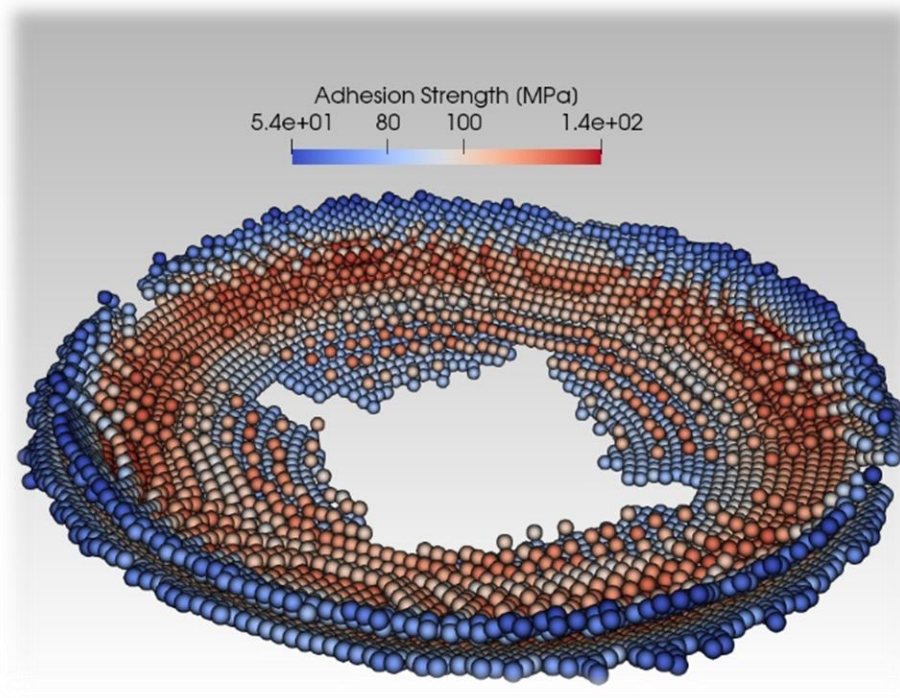*Figure 5.13 Distribution of adhesion strength in contact region. Combination of G_c and $\dot{G}_c$ being 1000 J/m² and 3.5 J/m²s respectively*

In Figure 5.14 the $\dot{G}_c$ value has further increased to 4.5 while maintaining G_c at 1000. The non-bonded area has increased extremly and can also be observed in the outer layer where bonding occures. The bonded area is relatively small and average adhesion strengh achieved was 13.41 MPa.

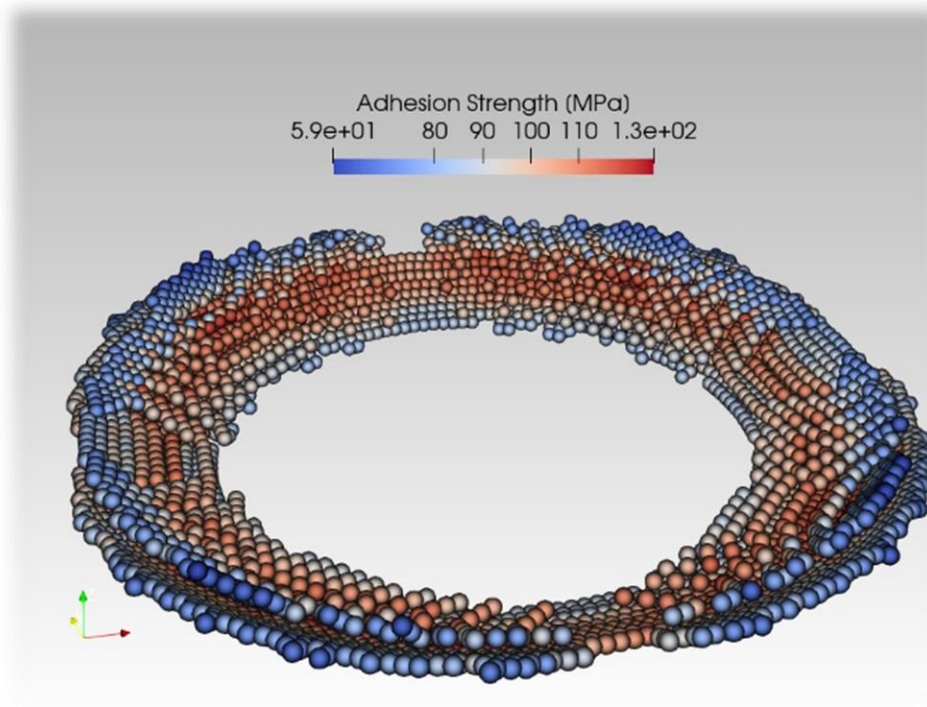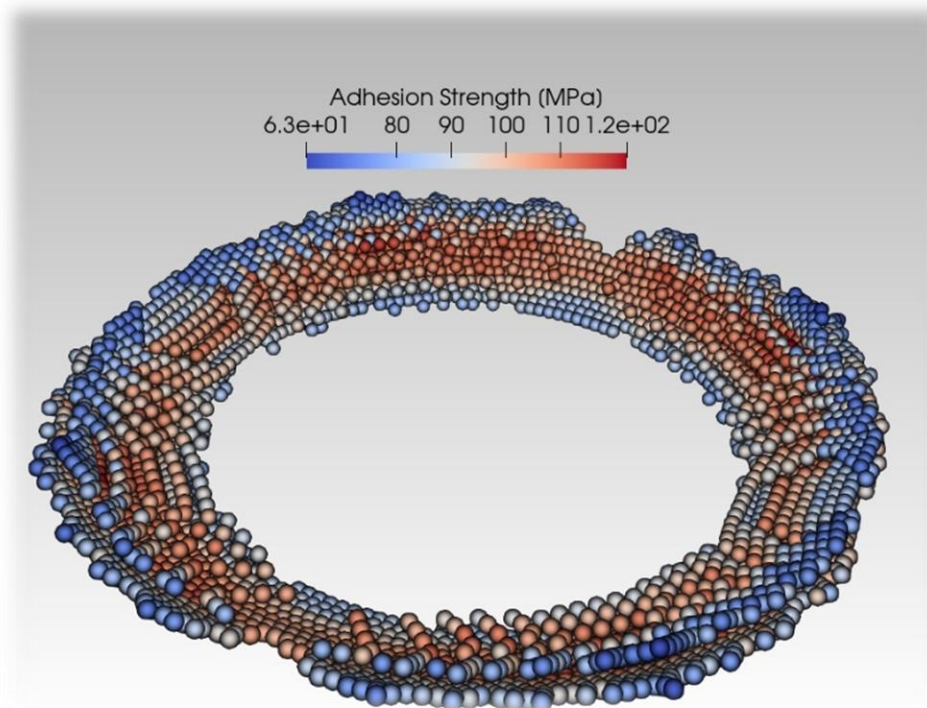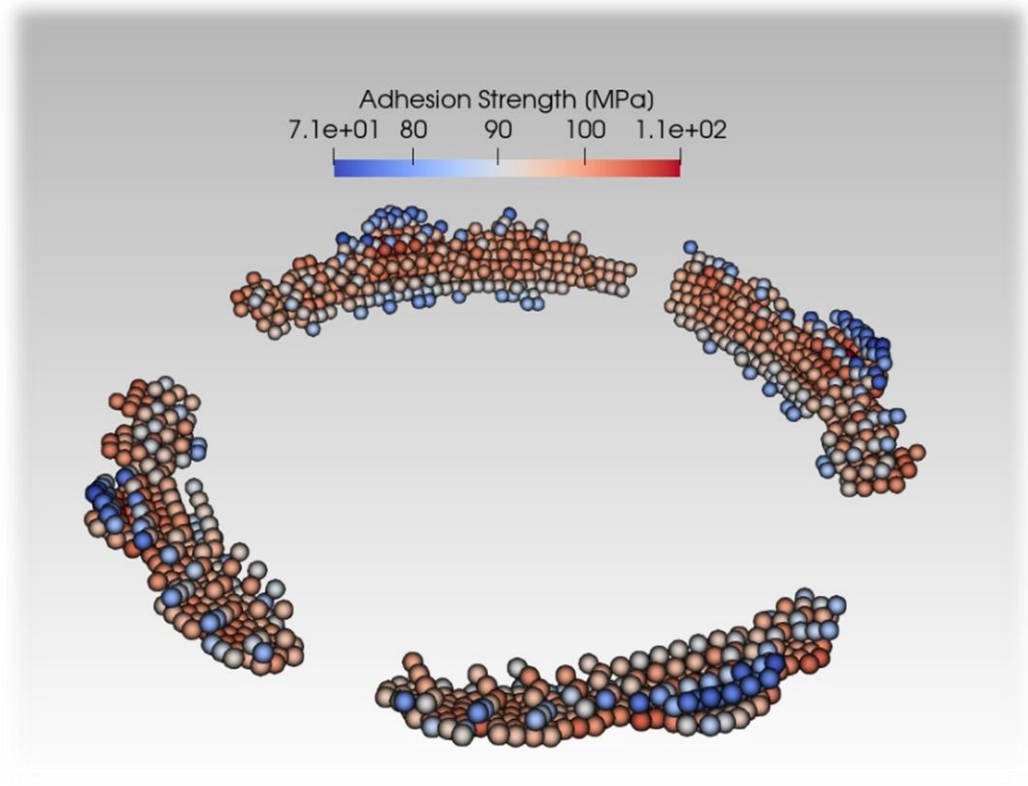*Figure 5.14 Distribution of adhesion strength in contact region. Combination of G_c and $\dot{G}_c$ being 1000 J/m^2 and 4.5 $J/m^2 s$ respectively*

Chapter 6: Conclusions and Future Work

This chapter will discuss the results obtained from chapter 5. The predicted adhesion strength as well as parameters influencing it are discussed. At the end of the chapter future works and further studies are mentioned.

6.1. Conclusions

First the dependence of the predicted adhesion strength on the bonding parameter D_{bond} is demonstrated in Figures 6.1 and 6.2. These two examples were taken from the results shown in Chapter 5. Figure 6.1 shows this correlation for $\dot{G}_c$ and G_c value being 4.5 J/m²s and 1000 J/m² respectively. Figure 6.2 shows this correlation for $\dot{G}_c$ and G_c value being 0.5 J/m²s and 1000 J/m² respectively.
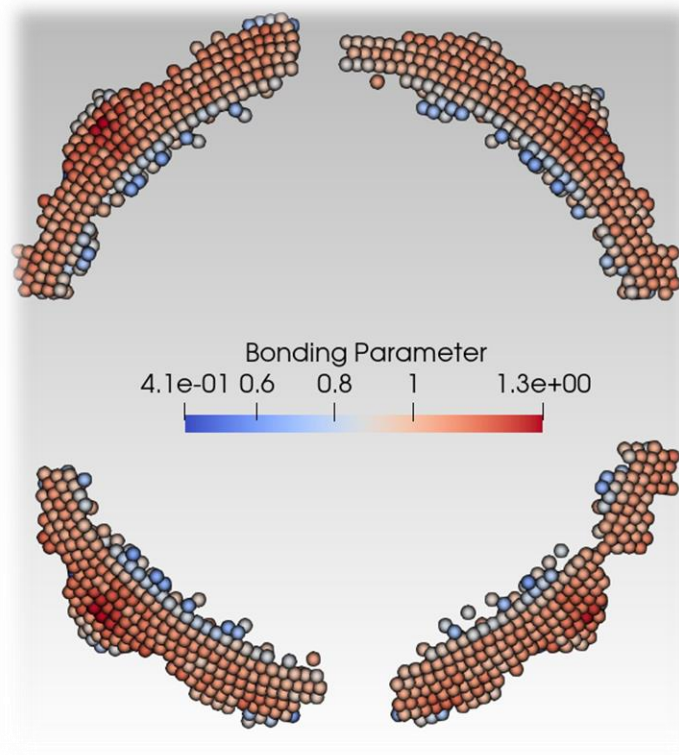
Figure 6.1 Quantitative comparison of the bonding parameter D distribution with the adhesion strength prediction distribution. ($\dot{G}_c$ and G_c value being 4.5 $J/m^2 s$ and 1000 J/m^2 respectively)
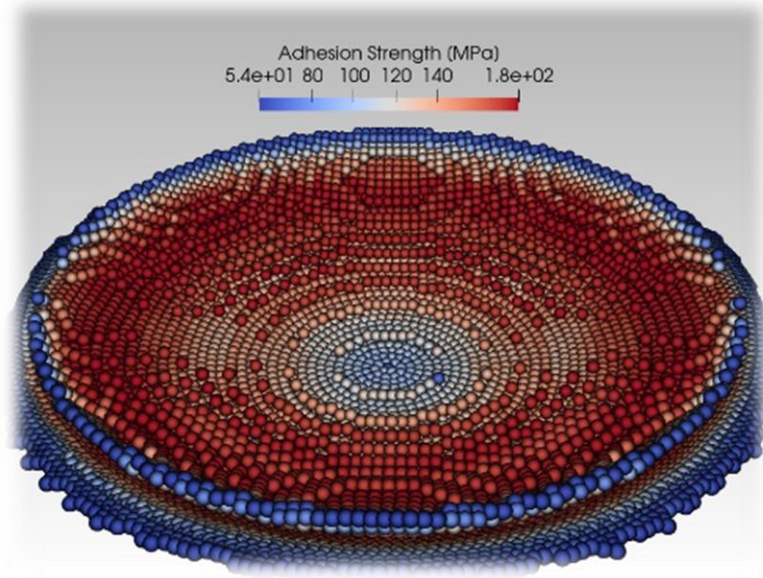
Figure 6.2 Quantitative comparison of the bonding parameter D distribution with the adhesion strength prediction distribution ($\dot{G}_c$ and G_c value being 0.5 J/m^2s and 1000 J/m^2 respectively)

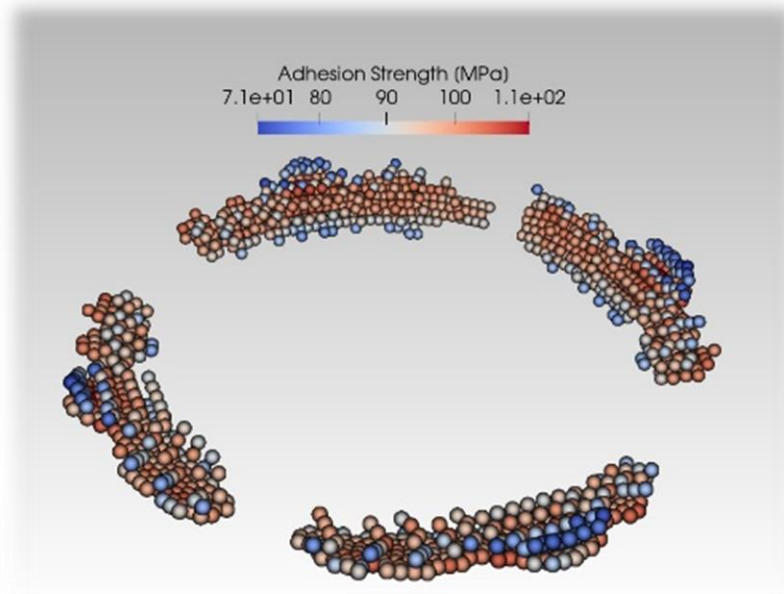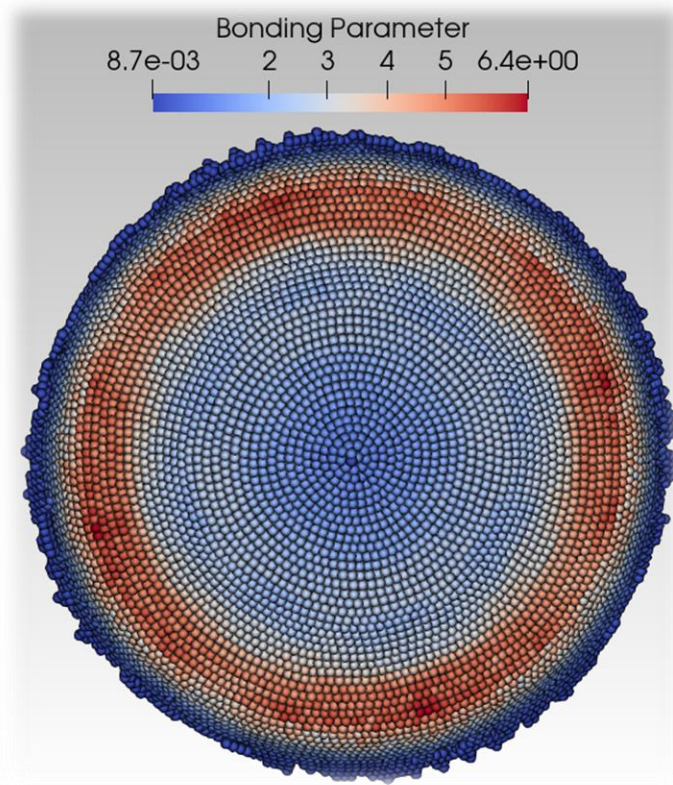It is observed that the variation of the predicted adhesion strength is consistent with the variation of the bonding parameters. The regions with minimum and maximum values of adhesion strength correspond to the regions with minimum and maximum values of bonding parameter.

Figure 6.3 shows the average adhesion strength achieved from all the tests in relation to the critical adhesion energy rate. As it was discussed earlier, since the increase of the critical adhesion energy resulted in increase of the non-bonded region in the contact area, the values for the average adhesion strength decrease with increasing the value of $\dot{G}_c$.

On the other hand, Figure 6.4 illustrates the relationship between the predicted adhesion strength and the critical adhesion energy, with a fixed value of the critical adhesion energy rate set at 1. It is observed that the predicted adhesion strength remains nearly unchanged with the variation of the critical adhesion energy.

The above results demonstrate that the rate of critical adhesion energy has a more significant impact on the predicted adhesion strength compared to critical adhesion energy. This implies that small variations or fluctuations in the rate of the critical adhesion energy can lead to significant differences in the predicted adhesion strength.

Figure 6.3 The predicted average adhesion strength plot for all 9 tests vs the critical adhesion energy rate

Figure 6.4 Predicted average adhesion strength vs critical adhesion energy, considering the critical adhesion energy rate set to 1
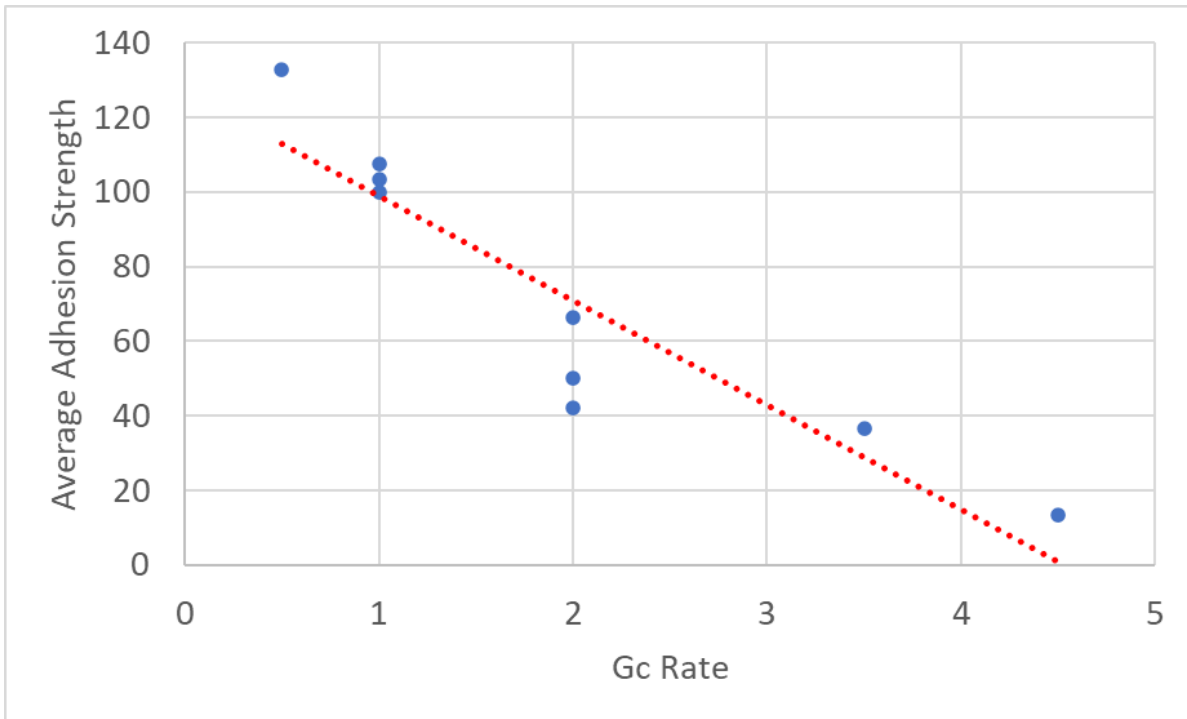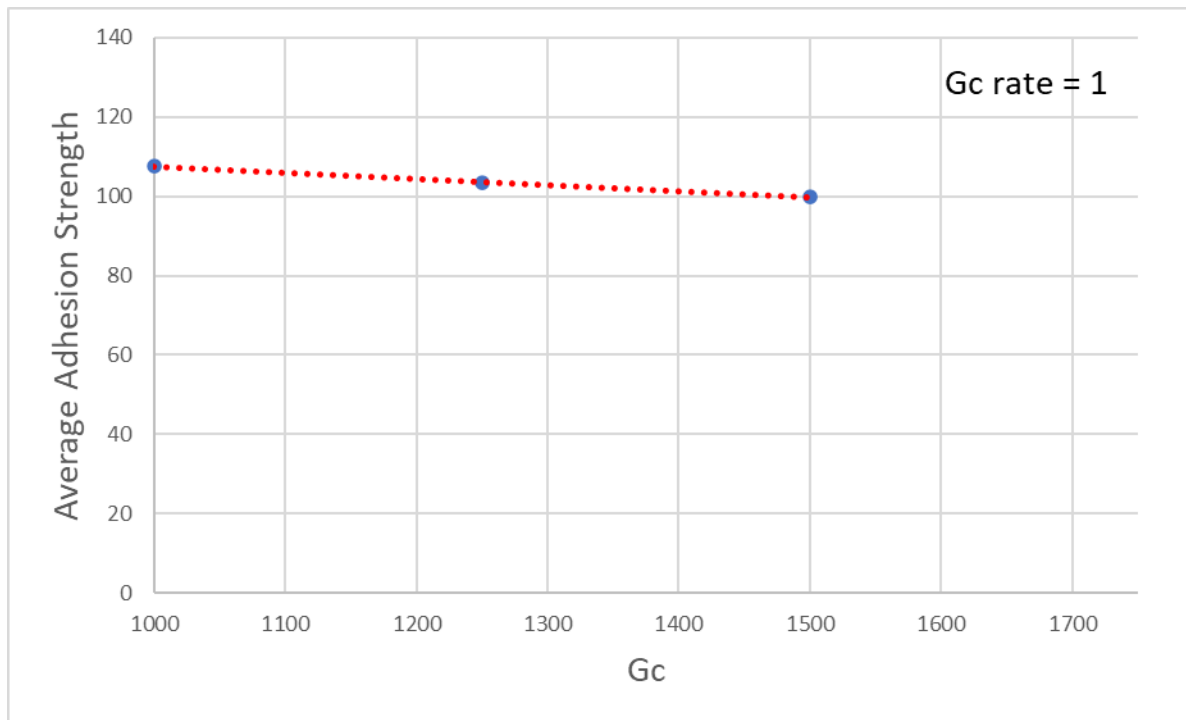
These tests show the effect of the change in materials properties can result in different values of bonding and in result the adhesion strength. Numerical study makes it much easier to observe these changes and analyze them in comparison to experimental studies. The numerical framework presented proves a reliable approach to analyzing the strength of bonding in particle impact in cold spray.

6.2. Future Work

As it was mentioned in chapter 5, κ and σ_c values were considered as trial values since the model should be calibrated. The σ_c value can be achieved by performing several adhesion tests and having an average value of the adhesion strength of the coating. Then the true value along with κ should also be obtained from calibrating the adhesion strength prediction model.

During the study of this thesis several tests were performed with one of the members of our research group. The attempt for single splat tests were made utilizing several relations from previous studies which correlated the pressure and temperature of the CS system with the particle velocity exiting the nozzle. The distance of the nozzle and the substrate was also studied to have optimal results of single splat tests. The attempted tests and the results obtained are yet to be concluded and achieved. In case of achieving the required coating of a single particle splat, an adhesion test can be performed to obtain the average adhesion strength.

In the previous study of our research group, the calibration formulation was developed and utilized in their study. Utilizing the tests conducted and studied in the above paragraph the parameters of the proposed relation for the prediction of the adhesion strength can be calculated (true values of κ and σ_c cand be obtained). The adhesion strength can then be calculated based on the estimated true values of the mentioned parameters.

Performing multiple particle impact simulations can resemble real world cases. The simulations performed for the study of this thesis can be performed utilizing several powder particles, as well as larger substrate to observe the bonding behavior of multi particle impacts. The material jetting of particles impacting the substrate and each other can be observed and analyzed. The adhesion strength can also be calculated and compared to single splat condition.

Different geometries can be considered while performing the simulations. An ideal shape can be considered for the prediction of the adhesion strength. The simulations of this study considered spherical particles and the jetting occurred at the periphery of the contact area which in the case of spherical particles is in circle form. Particles with other geometries can be considered and the deformation of the particle as well as the quality of the bonding can be analyzed and studied.

The current study can predict the bonding region, and how bonding shapes when particles impact the substrate. As it was mentioned earlier in the thesis, the south pole region was predicted and experimentally shown to be the nonbonded region, and the outer rim was considered to be the bonded region. The occurrence of the south pole has not been discussed considering numerical approach in the current study which can be further analyzed in future works.

References

[1]   Jonathan Tang, "Predictive model of impact-induced bonding in cold spray using the Material Point Method" *MASc Thesis*, (2021)

[2]   M. Reza Hirmand, Jonathan Tang, Hamid Jahed, "A numerical modelling framework for impact-induced bonding of powder particles in cold spray" *In submission*, (2022)

[3]   Victor Champagne Jr., Neil Matthews, Victor Champagne III, "Chapter Fourteen - Introduction to Supersonic Particle Deposition" *Aircraft Sustainment and Repair*, 799-844 (2018)

[4]   Xuemei Wang, Feng, Michael A. Klecka, Matthew D. Mordasky, Jacquelynn K. Garofano, Tahany El-Wardany, Aaron Nardi, Victor K. Champagne, "Characterization and modeling of the bonding process in cold spray additive manufacturing", *Additive Manufacturing 8*, 149–162 (2015)

[5]   Tobias Schmidt, Hamid Assadi, Frank Ga¨rtner, Horst Richter, Thorsten Stoltenhoff, Heinrich Kreye, and Thomas Klassen, "From Particle Acceleration to Impact and Bonding in Cold Spraying" *Journal of Thermal Spray Technology*, 794–808 (2009)

[6]   Harvinder Singh, Manoj Kumar, Rajdeep Singh, "An overview of various applications of cold spray coating process" *Volume 56*, Part 5, 2826-2830 (2022)

[7]   Sunday Temitope Oyinbo and Tien-Chien Jen, "Feasibility of numerical simulation methods on the Cold Gas Dynamic Spray (CGDS) Deposition process for ductile materials" *Manufacturing Rev. 7*, 24 (2020)

[8]   Wen Sun, Xin Chu, Haiming Lan, Renzhong Huang, Jibo Huang, Yingchun Xie, Jian Huang & Guosheng Huang, "Current Implementation Status of Cold Spray Technology: A Short Review", *Journal of Thermal Spray Technology volume 31*, 848–865 (2022)

[9]   Frank Gärtner, Thorsten Stoltenhoff, Tobias Schmidt & Heinrich Kreye, "The cold spray process and its potential for industrial applications" *Journal of Thermal Spray Technology volume 15*, 223–232 (2006)

[10]   Niraj Bala, Harpreet Singh, J. Karthikeyan, Satya Prakash, "Cold spray coating process for corrosion protection: A review" *Surface Engineering 30(6)*, 414-421 (2013)

[11]   Mohammad Diab, Xin Pang, Hamid Jahed, "The effect of pure aluminum cold spray coating on corrosion and corrosion fatigue of magnesium (3% Al-1% Zn) extrusion" *Surface and Coatings Technology Volume 309*, 15 January, 423-435 (2017)

[12]   Douglas E. Wolfe, Timothy J. Eden, John K. Potter & Adam P. Jaroh "Investigation and characterization of Cr3C2-based wear-resistant coatings applied by the cold spray process" *Journal of Thermal Spray Technology volume 15*, 400–412 (2006)

[13]   V. Champagne & D. Helfritch, "Critical Assessment 11: Structural repairs by cold spray" *Materials Science and Technology Volume 31*, Issue 6 (2015)

[14]   Shuo Yin, P. Cavaliere, Barry Aldwell, Richard Jenkins, Hanlin Liao, Wenya li, Rocco Lupoi, "Cold spray additive manufacturing and repair: Fundamentals and applications" *Additive Manufacturing 2*, 628-650 (2018)

[15]   Santosh Kumar, Neeru Jindal, Manoj Kumar, "Overview of cold spray coatings applications and comparisons: a critical review" *World Journal of Engineering*, 27–51 (2020)

[16]   W. Y. Li, D. D. Zhang, C. J. Huang, S. Yin, M. Yu ,F. F. Wang & H. L. Liao, "Modelling of impact behavior of cold spray particles: review", *Surface Engineering Volume 30*, Issue 5: Cold Spray Technology: Part I (2014)

[17]   J. Karthikeyan, "The advantages and disadvantages of the cold spray coating process, in: The cold spray materials deposition process", *Elsevier*, 62-71 (2007)

[18]   R. Ghelichi, D. MacDonald, S. Bagherifard, H. Jahed, M. Guagliano, B. Jodoin, "Microstructure and fatigue behavior of cold spray coated Al5052", *Acta Materialia 60*, 6555–6561 (2012)

[19]   Chang-Jiu Li, Wen-Ya Li, and Hanlin Liao "Examination of the Critical Velocity for Deposition of Particles in Cold Spraying" *Journal of Thermal Spray Technology*, 212-222 (2015)

[20]   D. Guo, M. Kazasidis, A. Hawkins, N. Fan, Z. Leclerc, D. MacDonald, A. Nastic, R. Nikbakht, R. Ortiz-Fernandez, S. Rahmati, M. Razavipour, P. Richer, S. Yin, R. Lupoi, B. Jodoin, "Cold Spray: Over 30 Years of Development Toward a Hot Future" *Journal of Thermal Spray Technology*, 866–907 (2022)

[21]   Kelvin Loke, Zhi-Qian Zhang, Sridhar Narayanaswamy, Pak Keng Koh, Vladimir Luzin, T. Gnaupel-Herold, Andrew Siao Ming Ang, "Residual Stress Analysis of Cold Spray Coatings Sprayed at Angles Using Through-thickness Neutron Diffraction Measurement" *Journal of Thermal Spray Technology*, 1810–1826 (2021)

[22]   Mostafa Hassani-Gangaraj, David Veysset, Keith A. Nelson, Christopher A. Schuh, "Impact-bonding with aluminum, silver, and gold microparticles: Toward understanding the role of native oxide layer", *Applied Surface Science* 528–532 (2019)

[23]   G. Bae, S. Kumar, S. Yoon, K. Kang, H. Na, H.-J. Kim, C. Lee, "Bonding features and associated mechanisms in kinetic sprayed titanium coatings", *Acta Mater*. 5654-5666 (2009)

[24]   Hamid Assadi, Frank Ga¨rtner, Thorsten Stoltenhoff, Heinrich Kreye, "Bonding mechanism in cold gas spraying" *Acta Materialia* 4379–4394 (2003)

[25]   Mostafa Hassani-Gangaraj, David Veysset, Victor K. Champagne, Keith A. Nelson, Christopher A. Schuh, "Adiabatic shear instability is not necessary for adhesion in cold spray", *Acta Materialia* 430-439 (2018)

[26]   S.I. Imbriglio, M. Hassani-Gangaraj, D. Veysset, M. Aghasibeig, R. Gauvin, K.A. Nelson, C.A. Schuh, R.R. Chromik, "Adhesion strength of titanium particles to alumina substrates: A combined cold spray and LIPIT study" *Surface & Coatings Technology* 403–412 (2019)

[27]   A. Nastic, M. Vijay, A. Tieu, S. Rahmati, B. Jodoin, "Experimental and Numerical Study of the Influence of Substrate Surface Preparation on Adhesion Mechanisms of Aluminum Cold Spray Coatings on 300M Steel Substrates", *Journal of Thermal Spray Technology* 1461–1483 (2017)

[28]   Dina Goldbaum, J. Michael Shockley, Richard R. Chromik, Ahmad Rezaeian, Stephen Yue, Jean-Gabriel Legoux, and Eric Irissou "The Effect of Deposition Conditions on Adhesion Strength of Ti and Ti6Al4V Cold Spray Splats", *Journal of Thermal Spray Technology* 288–303 (2021)

[29]   Xu Song, Xiao-Zhe Jin, Wei Zhai, Adrian Wei-Yee Tan, Wen Sun, Feng Li, Iulian Marinescu, Erjia Liu, "Correlation between the macroscopic adhesion strength of cold spray coating and the microscopic single-particle bonding behaviour: Simulation, experiment and prediction" *Applied Surface Science* 149-165 (2021)

[30]   B. Yildirim, H. Fukanuma, T. Ando, A. Gouldstone, S. Muftu, "A numerical investigation into cold spray bonding processes", *Journal of Tribology* 011-102 (2015)

[31]   W. Li, K. Yang, D. Zhang, X. Zhou, X. Guo, "Interface behavior of particles upon impacting during cold spraying of Cu/Ni/Al mixture" *Materials & Design* 237-246 (2016)

[32]   W.Y. Li, C. Zhang, C. J. Li, H. Liao, Modeling aspects of high velocity impact of particles in cold spraying by explicit finite element analysis, *Journal of Thermal Spray Technology* 921-933 (2009)

[33]   Daniel Nelias, Jing Xie, Hélène Walter-Le Berre, Yuji Ichikawa, Kazuhiro Ogawa "Simulation of the Cold Spray Deposition Process for Aluminum and Copper using Lagrangian, ALE and CEL Methods" *Thermo-Mechanical Industrial Processes Edition: 1 Chapter: 7* (2014)

[34]   A. Manap, T. Okabe, K. Ogawa, "Computer simulation of cold sprayed deposition using smoothed particle hydrodynamics" *Procedia Engineering 10*, 1145-1150 (2011)

[35]   A. Joshi, S. James, Molecular dynamics simulation study on effect of process parameters on coatings during cold spray process, *Procedia Manufacturing 26*, 190-197 (2018)

[36]   Xiong Zhang, Zhen Chen, Yan Liu, "The Material Point Method, A Continuum-Based Particle Method for Extreme Loading Cases" *Published by Elsevier Inc.* (2017)

[37]   D. Helfritch, V. Champagne, "A Model Study of Powder Particle Size Effects in Cold Sray Deposition", *U.S. Army Research Laboratory, Aberdeen Proving Ground, MD* (2008)

[38]   Shuo Yin, Xinkun Suo, Jiaqing Su, Zhiwei Guo, Hanlin Liao, and Xiaofang Wang, "Effects of Substrate Hardness and Spray Angle on the Deposition Behavior of Cold-Sprayed Ti Particles", *Journal of Thermal Spray Technology 76–83* (2013)

[39]   https://www.youtube.com/watch?v=WoAQSy4iGmk, *15 April* (2023)

[40]   G. Johnson and W. Cook, "A constitutive model and data for metals subjected to large strains, high strain rates, and high temperatures". *Proc. 7th Int. Symposium on Ballistics* 541 (1983)

[41]   Gaurav Singh, Purnashis Chakraborty, Vikrant Tiwari, "Constitutive Behavior of a Homogenized AT61 Magnesium Alloy under Different Strain Rates and Temperatures: An Experimental and Numerical Investigation", *Journal of Materials in Civil Engineering Volume 35*, Issue 9 (2023)

[42]   M. NIKKHAH, F. HONARVAR, E. DEHGHAN, "Elastodynamic solution for plane-strain response of functionally graded thick hollow cylinders by analytical method" *Appl. Math. Mech. -Engl. Ed., 32(2)*, 189–202 (2011)

[43]   Adrian Wei-Yee Tan, Wen Sun, Ayan Bhowmik, Jun Yan Lek, Iulian Marinescu, Feng Li, Nay Win Khun, Zhili Dong, Erjia Liu, "Effect of coating thickness on microstructure, mechanical properties and fracture behaviour of cold sprayed Ti6Al4V coatings on Ti6Al4V substrates" *Surface & Coatings Technology 349*, 303–317 (2018)

[44]   R. Drehmann, T. Grund, T. Lampke, B. Wielage, C. Wu¨stefeld, M. Motylenko D. Rafaja. "Essential Factors Influencing the Bonding Strength of Cold-Sprayed Aluminum Coatings on Ceramic Substrates" *Journal of Thermal Spray Technology 27*, 446–455 (2018)

[45]   R. Huang, H. Fukanuma, "Study of the Influence of Particle Velocity on Adhesive Strength of Cold Spray Deposits" *Journal of Thermal Spray Technology 21*, 541–549 (2011)

[46]   Venkata Naga Vamsi Munagala, Sara I. Imbriglio, Richard R. Chromik, "The influence of powder properties on the adhesion strength and microstructural evolution of cold sprayed Ti6Al4V single splats" *Materials Letters* 244, 58–61 (2019)

[47]   Mostafa Hassani-Gangaraj, David Veysset, Keith A. Nelson, Christopher A. Schuh, "In-situ Observations of Single Micro-particle Impact Bonding", *Scripta Materialia*. 145, 9-13 (2018)

[48]   Ahmed Fardan, Christopher C. Berndt, Rehan Ahmed, "Numerical modelling of particle impact and residual stresses in cold sprayed coatings: A review" *Surface & Coatings Technology 409*, 126-835 (2021)

[49]   C.D. Reddy, Zhi-Qian Zhang, S. Msolli, Junyan Guo, N. Sridhar, "Impact induced metallurgical and mechanical interlocking in metals" *Computational Materials Science 192*, 110-363 (2021)

[50]   Ahmad Nourian, Tricia Schwartz, Samuel Boese, Sinan Muftu, "Effects of Process Parameters on Cold Spray Deposition of Al-6061 Alloy" *J Thermal Spray Tech 31*, 2517–2536 (2022)

[51]   R. Singh, S. Schruefer, S. Wilson, J. Gibmeier, R. Vassen, "Influence of coating thickness on residual stress and adhesion-strength of cold-sprayed Inconel 718 coatings" Surface & Coatings *Technology 350*, 64–73 (2018)